KINK–ANTIKINK INTERACTIONS IN THE DOUBLE SINE-GORDON EQUATION

David K. CAMPBELL
Center for Nonlinear Studies and Theoretical Division, Los Alamos National Laboratory Los Alamos, NM 87545, USA

Michel PEYRARD
Laboratoire d'Optique du Réseau Cristallin, Faculté de Sciences, Université de Dijon, 21100 Dijon, France

Pasquale SODANO*
Dipartimento di Fisica Teorica e S.M.S.A. Università di Salerno, I 84100, Salerno, Italy and Sezione di Napoli I.N.F.N., I 80138, Napoli, Italy

We study numerically the interactions of a kink (K) and an antikink ($\overline{\text{K}}$) in the double sine-Gordon equation with potential $V(\phi) = -4[-\cos(\phi/2) + \eta \cos \phi]/[1 + |4\eta|]$. As a function of initial velocity in the K$\overline{\text{K}}$ collisions, we observe and analyze quantitatively a rich structure of "resonances" in most ranges of η.

1. Introduction

Among the *non*-integrable models used to describe nonlinear phenomena in real quasi-one-dimensional physical systems, one of the most frequently occurring is the "double sine-Gordon" [DSG] equation. In this model, a real scalar field $\phi(x, t)$ satisfies an equation of the form [1]

$$\frac{\partial^2 \phi(x,t)}{\partial t^2} - \frac{\partial^2 \phi(x,t)}{\partial x^2} + \frac{2}{1 + |4\eta|}$$

$$\times \left[-\sin \frac{\phi(x,t)}{2} + 2\eta \sin \phi(x,t) \right] = 0, \quad (1.1)$$

where η is a parameter ($-\infty < \eta < \infty$) that is determined by the physical system being modelled and the specific choices of signs and constant factors in (1.1) have been made for later convenience [1].

This equation follows from the Hamiltonian field theory described by

$$H = \int dx \left[\frac{1}{2} \left(\frac{\partial \phi}{\partial t} \right)^2 + \frac{1}{2} \left(\frac{\partial \phi}{\partial x} \right)^2 + V(\phi) \right], \quad (1.2)$$

*C.T.P. 6/408, MIT, Cambridge, MA 02139, USA.

where the potential $V(\phi)$ is given by [1]

$$V(\phi) = -\frac{4}{1 + |4\eta|} \left[-\cos \frac{\phi}{2} + \eta \cos \phi \right]. \quad (1.3)$$

As η is varied over the range $-\infty < \eta < \infty$, this potential exhibits a variety of structures. Although in later sections we shall discuss these different structures in some detail [2], it is important here to provide a qualitative feeling for them. Clearly, for $\eta \to \pm \infty$, $V(\phi)$ reduces to a sine-Gordon [SG] form for ϕ, while for $\eta = 0$, it leads to a SG form for $\phi/2$. Thus in both these limits the familiar sine-Gordon solitons – kinks and breathers – will occur as spatially localized, nonlinear excitations in the physical systems being modelled. The behavior of $V(\phi)$ for general η can usefully be divided into four regions [2] as shown in figs. 1a–d. In region I, defined by $\eta < -\frac{1}{4}$ (fig. 1a), the potential has two distinct types of minima, degenerate in energy and separated by inequivalent barriers. Recalling that topological "kink" solitons connect adjacent degenerate minima of the potential, we see that there are two different types of kinks in this region. In regions II (fig. 1b) and II'
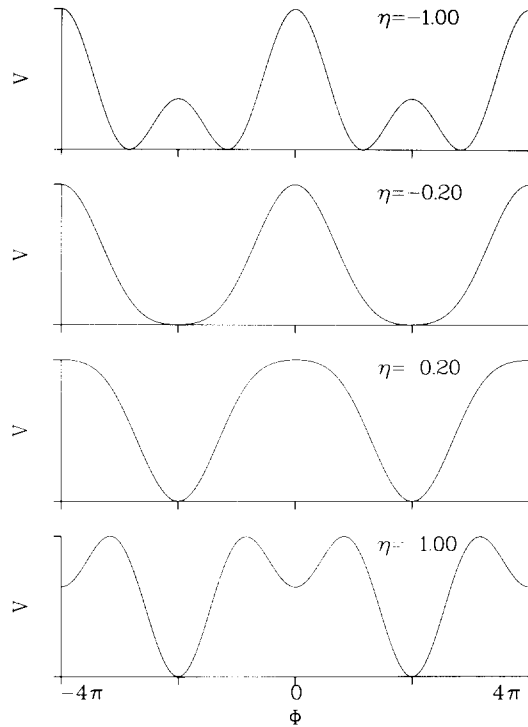
Fig. 1. A plot of the potential $V(\phi) = -4/(1 + |4\eta|)$ $\times(-\cos\phi/2 + \eta\cos\phi)$ showing its characteristic structure in each of the four distinct regions in η. a) Region I: For $\eta < -\frac{1}{4}$ (here we have chosen $\eta = -1.00$), the potential has two distinct types of minima, degenerate in energy and separated by inequivalent barriers. Thus there exist two types of topological kinks. b) Region II: For $-\frac{1}{4} < \eta < 0$ (here we have chosen $\eta = -0.20$) the potential has broad minima separated by narrow barriers. There exists one type of topological kink. c) Region II': For $0 < \eta < \frac{1}{4}$ (here we have chosen $\eta = +0.20$) the potential has narrow minima separated by broad barriers. There exists one type of topological kink. d) Region III: For $\eta > \frac{1}{4}$ (here we have chosen $\eta = +1.00$) the potential has two distinct types of minima but they are non-degenerate except for $\eta \to \infty$. Thus there exists only one type of topological kink.

(fig. 1c), defined by $-\frac{1}{4} < \eta < 0$ and $0 < \eta < \frac{1}{4}$, respectively, the potential has a single type of minima, is thus structurally similar to the pure SG potential, and has a single type of kink soliton. We distinguish between these two regions for later convenience. In region III (fig. 1d), defined by $\frac{1}{4} < \eta$, there are two distinct types of minima for the potential, but they are not degenerate except for $\eta \to \infty$. Thus for finite η there exists one type of topological kink, but, as $\eta \to \infty$, it in effect splits into two separate and independent kinks.

Importantly, particularly given the variety of possible structures of $V(\phi)$, the values of η that arise in actual physical situations cover essentially the whole possible range. In the B phase of superfluid ^{3}He, kink soliton solutions to (1) can be viewed as the boundary (domain wall) between two different homogeneous textures; for this application, $\eta = -1$ [3–5].

The phenomenon of self-induced transparency in a two-level system in which each of the levels has a five-fold degenerate structure has also been modelled by the DSG, but with $\eta = +1$ [5–8]. In this application, experiments on sodium vapor [8] have confirmed qualitatively theoretical expectations based on the DSG model.

Magnetic systems with low effective dimension have also been modelled by (1.1). For ferromagnetic Heisenberg spin chains, the DSG can arise when effects of single-ion or exchange anisotropies or applied magnetic fields are considered [9–11]. Further, when the coupling between magnons and their induced dipolar electromagnetic field is included, a DSG model can be derived to describe solitary waves related to "polaritons" [12]. In these applications, depending on the values of anisotropies and applied or induced fields, essentially all values of η are possible. In *anti*ferromagnetic Heisenberg chains, both Ising-like single ion anisotropies [11] and Dzyaloshinski–Moriya antisymmetric exchange interactions [13] can lead to the DSG equations. In each of these cases, the relevant regime is $\eta \gtrsim 1$. Again, there are experimentally accessible systems – CsNiF$_3$ in the ferromagnetic case [14], and (CH$_3$)$_4$NMnCl$_3$ (called TMMC in the literature [15]) in the antiferromagnetic case – to which the DSG description can be compared.

In the rapidly growing area of commensurate-incommensurate (C–IC) phase transitions [16], the DSG equation has arisen in several contexts. Apart from general studies aimed at clarifying the nature of the (C–IC) phase transition [17, 18], the DSG equation has been derived as a model for the influence of an external electric field on the C–IC transition in the improper ferroelectrics K$_2$SeO$_4$

and $(NH_4)_2BeF_4$ [19] and as a description of the spin density wave properties of the material $(TMTSF)_2PF_6$ at ambient pressure [20]. In both these physical applications, a wide range of values of η – both positive and negative – is accessible, depending on the externally applied fields.

A physical application that relies on the *propagating* nature of the kink solutions to (1.1) has been suggested [21] in the context of the piezoelectric long chain polymer PVF_2 (polyvinylidene fluoride), which has the chemical formula $(-CH_2-CF_2-)_n$, with n large. In the presence of an external field, the large electric dipole moments associated with the CF_2 units can be aligned. The dynamics of this process, which is called poling, has been modelled [21] by the propagation of a kink soliton down the length of the chains.

Most of these studies have focused on the nature, properties, and physical interpretation of the static solitary wave solutions to the classical field equation, (1.1). However, in many of the applications, the thermodynamics has also been investigated [2, 10, 12, 19, 22] and a study of the relation of the *quantum* double sine-Gordon system to an eight–vertex model in an external electric field has also been made [23]. Further, a number of authors have investigated, both analytically and numerically, several aspects of the *dynamics* of the solitary wave solutions to (1.1), including the evolution of individual solitary waves from various initial conditions [4–7, 24] the nature of uniformly translating solitary waves in damped DSG systems [25, 26], and the properties of kink–antikink ($K\overline{K}$) interactions in these systems [4–5, 27, 28].

Apart from indicating clearly that the DGS model is *not* a completely integrable system, these dynamical studies have revealed a number of tantalizing features, including the trapping of kink and antikink to form a localized, long-lived breather state [4–5, 27, 28], conversion between different types of kinks (for $\eta < -\frac{1}{4}$) [4–5, 27–28], and the existence of "wobbling" kink solutions (for $\eta > \frac{1}{4}$) [4–5, 7, 29]. Given the broad physical relevance of the DSG model, it seems clear that a systematic numerical study of the DSG dynamics,

extending this earlier work and leading hopefully to an intuitive and quantitative theoretical interpretation, would be valuable.

Accordingly, in the present paper we have begun such a study, focusing on the problem of $K\overline{K}$ interactions in the DSG equation for several representative values of η in the range $-\infty < \eta < \infty$. This investigation follows naturally from our previous papers [30, 31] – hereafter referred to as CSW and PC, respectively – on kink interactions in non-integrable field theories, and we will discover that the theoretical concepts introduced in CSW and PC – in particular, the importance of the nature of the small oscillations around individual kinks and the "resonant energy exchange mechanism" [30, 31] – permit a *quantitative* interpretation of our results for most values of η. In addition, for certain values of η, we observe qualitatively new phenomena – for example, the formation of two counterpropagating "breathers" as the final state of a $K\overline{K}$ interaction – which we are able to interpret qualitatively within our theoretical framework.

The remainder of the paper is organized into five sections. In section 2 we review briefly the explicit forms of the kink solutions for the different regimes in η and discuss the small oscillations around these solutions. In section 3 we study the range $\eta < -\frac{1}{4}$, in which there exist two types of kink solitons. To complement previous numerical work [4–7, 27–28], we focus primarily on the interactions of the "small" kinks [2, 22] and demonstrate the existence of resonances in $K\overline{K}$ scattering both for $\eta = -\frac{1}{2}$ and $\eta = -1$. In addition to the "two-bounce" resonances familiar from CSW and PC, we exhibit several "multi-bounce" resonances, as expected from our earlier general theoretical considerations but not previously studied systematically. We develop an explicit theory of these higher bounce resonances and find that it provides a quantitative explanation of our data. In section 4, we consider the region $-\frac{1}{4} < \eta < 0$, in which the potential is topologically similar to the SG potential and for which there is only one type of kink. Since in the small oscillations around this

kink there is no internal shape mode, we expect no resonances in $K\overline{K}$ scattering. Our numerical results confirm this expectation, and in addition show a qualitative difference between the trapped $K\overline{K}$ find states for $-\frac{1}{4} > \eta \geq -1/16$ and $-\frac{1}{16} \leq \eta < 0$. We explain this behavior by an analytic estimate of the allowed region in η for the existence of a stable "breather" solution to (1.1). In section 5 we investigate the region $\eta > 0$. Introducing a new parameter, R, such that $\eta \equiv \sinh^2 R/4$, and following previous work [5, 19, 32, 33], we show that the 2π kink soliton of (1.1) in the variable $\phi/2$ can usefully be viewed, for large R, as a bound state of two solitons (separated by a distance R) of the SG equation that holds for ϕ as $\eta \to \infty$. We examine numerically and analytically the consequences of this decomposition [33] for $K\overline{K}$ collisions and demonstrate that (again for large R) one possible final state of these interactions is two counterpropagating "breathers". We summarize our principal results and discuss their implications in section 6.

2. Isolated kink solutions and small oscillations

Although the properties of the DSG potential and its isolated kink solutions have been extensively studied and recorded in the literature, given the bewildering array of conventions, prudence requires that we summarize the relevant results here in our notation. As defined by (1.2) and depicted in fig. 1, the DSG potential has period 4π in ϕ and has extrema at $\phi = 2n\pi$ and $\phi = 4m\pi \pm \phi_0$, with $\phi_0 \equiv 2\cos^{-1}(1/4\eta)$ and n, m integers; clearly, the latter extrema exist only for $|\eta| > \frac{1}{4}$. As η varies, the nature of these extrema changes. One finds (see also fig. 1)

1) for $\eta < -\frac{1}{4}$, the values $\phi = 2n\pi$ are maxima, whereas $\phi = 4m\pi \pm \phi_0$ are minima;

2) for $|\eta| < \frac{1}{4}$, the values $\phi = 2n(2\pi)$ are maxima, whereas those at $\phi = (2n + 1)2\pi$ are minima; and

3) for $\eta > \frac{1}{4}$, the values at $\phi = 2n\pi$ are minima

(for n even, they are local minima, for n odd, global), and those at $\phi = 4m\pi \pm \phi_0$ are maxima.

The solutions for small oscillations about the minima of the potential are plane waves, satisfying the dispersion relation

$$\omega(k) = \left(\omega_0^2(\eta) + k^2\right)^{1/2},$$

with

$$\omega_0(\eta) = [(|4\eta| - 1)/|4\eta|]^{1/2} \tag{2.1}$$

for $\eta < -\frac{1}{4}$ and $\omega_0(\eta) = [(1 + 4\eta)/(1 + |4\eta|)]^{1/2}$ for $\eta > -\frac{1}{4}$. The behavior of $\omega_0(\eta)$ versus η is sketched in fig. 2.

Since (stable) kink solutions interpolate between adjacent (global) minima of the potential, we see that for $\eta < -\frac{1}{4}$, there exist two different types of kinks. The corresponding static solutions are (1) the "small" kink (antikink), $\phi^I_{K(\overline{K})}$, interpolating between ϕ_0 and $4\pi - \phi_0 \pmod{4\pi}$ and given by

$$\phi^I_{K(\overline{K})}(x) = (2n + 1)2\pi$$

$$\pm 4\tan^{-1}\left[\left(\frac{|4\eta| - 1}{|4\eta| + 1}\right)^{1/2} \tanh\left(\frac{|4\eta| - 1}{16|n|}\right)^{1/2} x\right], \tag{2.2a}$$

where $(+)$ refers to kink (K) and $(-)$ to antikink $(\overline{K})$. The energy of the static kink is

$$E^I_{K(\overline{K})} = \left(\frac{4}{1 + 4|\eta|}\right)^{1/2} \frac{2}{\sqrt{|\eta|}}$$

$$\times \left[(16\eta^2 - 1)^{1/2} + \frac{\phi_0}{2} - \pi\right]; \tag{2.2b}$$

and (2) the "large" kink (antikink), $\phi^{II}_{K(\overline{K})}$, interpolating between $-\phi_0$ and $\phi_0 \pmod{4\pi}$ and given by

$$\phi^{II}_{K(\overline{K})}(x) = (2n)2\pi$$

$$\pm 4\tan^{-1}\left[\left(\frac{|4\eta| + 1}{|4\eta| - 1}\right)^{1/2} \tanh\left(\frac{|4\eta| - 1}{|16\eta|}\right)^{1/2} x\right], \tag{2.3a}$$
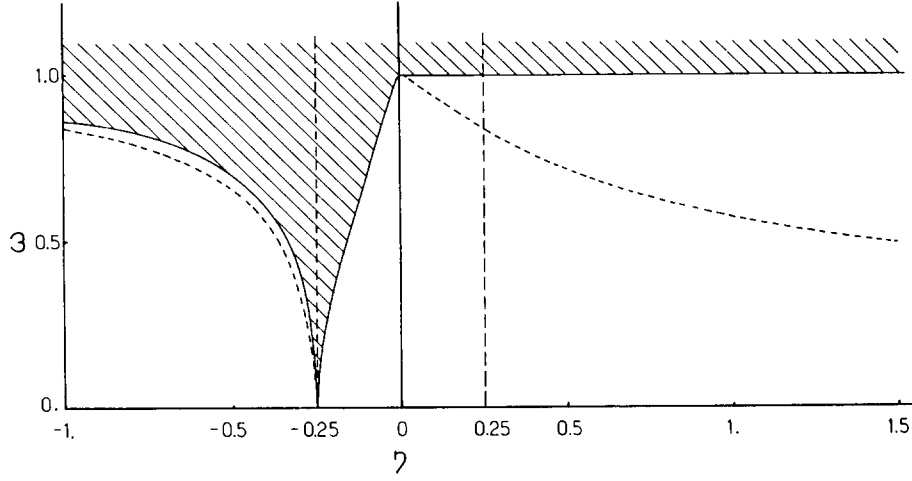
Fig. 2. A plot showing the spectrum of small oscillations versus η for the DSG. The continuum, shown as a shaded region, exists for linear oscillations both about the ground states and about the kinks. The dashed line below the continuum corresponds to the localized shape mode of a kink and exists only for $\eta < -\frac{1}{4}$ and $\eta > 0$. Note that for $\eta < -\frac{1}{4}$ the shape mode exists *only* around the small kink solution.

where again $+(-)$ refers to $K(\overline{K})$. The energy of this static kink is

$$E_{K(\overline{K})}^{II} = \left(\frac{4}{1+4|\eta|} \right)^{1/2} \frac{2}{\sqrt{|\eta|}} \left[(16\eta^2 - 1)^{1/2} + \frac{\phi_0}{2} \right].$$

(2.3b)

In both (2.2b) and (2.3b) $\phi_0 = 2\cos^{-1}(1/4\eta)$. In fig. 3 we display these solutions, together with the DSG potential, for $\eta = -1.00$. For $\eta > -\frac{1}{4}$, there is only one type of kink, $\phi_{K(\overline{K})}(x)$, interpolating between -2π and 2π (mod 4π) and having the form

$$\phi_{K(\overline{K})}(x) = (2n)2\pi$$

$$\pm 4\tan^{-1}\left[\left(\frac{1}{(1+4\eta)} \right)^{1/2} \sinh\left(\frac{1+4\eta}{1+|4\eta|} \right)^{1/2} x \right],$$

(2.4a)

where as usual $+(-)$ refers $K(\overline{K})$. The energy of this solution is

$$E_{K(\overline{K})} = \left(\frac{4}{1+4|\eta|} \right)^{1/2} \frac{4}{\sqrt{|\eta|}}$$

$$\times \left[2\sqrt{|\eta|}\,(1+4\eta)^{1/2} + \sin^{-1} 2\sqrt{|\eta|} \right]$$

(2.4b)

for $-\frac{1}{4} < \eta \leq 0$ and

$$E_{K(\overline{K})} = \left(\frac{4}{1+4|\eta|} \right)^{1/2} \frac{4}{\sqrt{\eta}} \left[2\sqrt{\eta}\,(1+4\eta)^{1/2} \right.$$

$$\left. + \ln\left(2\sqrt{\eta} + (1+4\eta)^{1/2} \right) \right]$$

(2.4c)

for $\eta \geq 0$.

From the form of these kink solutions, as well as from the form of $\omega_0(\eta)$, shown in (2.1) we see that the value $\eta = -\frac{1}{4}$ is a special point [34]. From (2.2) and (2.3) it is straightforward to see that as $\eta \to -\frac{1}{4}$ from below, the "small" kink goes smoothly to one of the minima of the potential (and $E^I \to 0$) whereas the "large" kink goes smoothly to the correct kink solution for $\eta = -\frac{1}{4}$,

$$\phi_{K(\overline{K})}^{(1/4)} \equiv (2n)2\pi \pm \tan^{-1} x/\sqrt{2},$$

(2.5a)

with energy

$$E^{(1/4)} = 4\sqrt{2}\,\pi.$$

(2.5b)

Similarly, as $\eta \to -\frac{1}{4}$ from above, the solution (2.4) for $\eta > -\frac{1}{4}$ goes smoothly to (2.5).

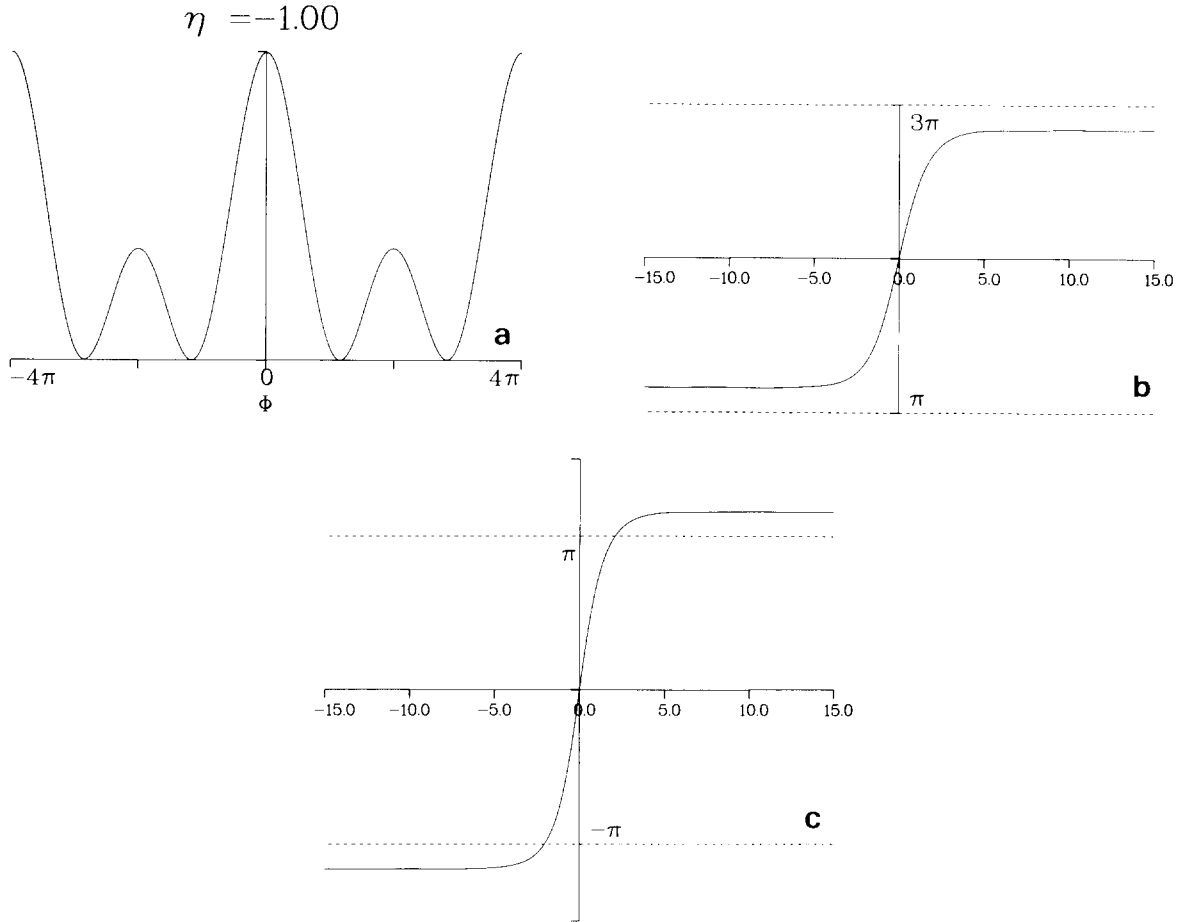Since the small oscillations about the kink solutions play a major role in our interpretation of $K\overline{K}$

$$\eta = -1.00$$

Fig. 3. A plot for $\eta = -1.00$ of a) the DSG potential; b) the "small" kink solution, $\phi_K(x)$; and c) the "large" kink solution, $\phi_K^{II}(x)$.

scattering [30, 31], we conclude this section by discussing them. The linearized oscillations about the static kinks obey an equation of the form

$$\frac{-d^2\psi(x)}{dx^2} + V_{SCH}(x)\psi(x) = \omega^2\psi(x), \qquad (2.6)$$

where $\psi(x) \equiv \phi(x) - \phi_K(x)$, with $\phi_K(x)$ the particular kink or antikink solution under considera tion and

$$V_{SCH}(x) \equiv \frac{d^2V(\phi)}{d\phi^2}\bigg|_{\phi=\phi_K(x)} \qquad (2.7)$$

The notation $V_{SCH}(x)$ is chosen because (2.6) has the form of a Schrödinger equation in one-dimen-

sional quantum mechanics; we shall find this analogy useful in interpreting the small oscillations. Although one can, using the kink solutions, write an explicit expression for V_{SCH}, the resulting equation does not, for general η, admit a useful analytic solution [22]. Thus, following previous work [22], we have solved (2.6) numerically for each value of η we have studied. The results, which are sketched in fig. 2, show that, for all η, (2.6) admits a continuum of plane wave solutions starting at $\omega = \omega_0(\eta)$, with $\omega_0(\eta)$ given by (2.1). In addition, one finds localized solutions to (2.6), corresponding, in the language of quantum mechanics, to states "bound" to the kink. First, for each of the kink solutions listed above, there is the well-known

"Goldstone" mode, having $\omega = 0$ and $\psi(x) = d\phi_K(x)/dx$, where $\phi_K(x)$ is the particular kink being considered. As is familiar, these modes arise because the translation invariance of the theory is broken by choosing a particular location for the kink. Second, for $\eta < -\frac{1}{4}$, one finds for the "small" kink an additional localized mode, with $\omega \equiv \omega_s \neq 0$, which can be viewed as an "internal" oscillation of the shape of the kink [29–31]. As in CSW and PC, we shall refer to this as a shape mode. Its location is illustrated in fig. 2. Importantly, there is *no* such shape mode for the large kink. Similarly, for the kink in the region $-\frac{1}{4} < \eta < 0$, there is no shape mode. For $\eta > 0$, however, the shape mode is again present; as is shown in fig. 2, for $\eta \rightarrow +\infty$, $\omega_s \rightarrow 0$. We shall present an interpretation of this result in section 5.

With our summary of single kink properties now complete, we need only to describe the numerical method used to study the $K\overline{K}$ interactions before turning to our results. As in PC, our numerical scheme involves using a fourth-order Runge-Kutta algorithm for solving the Newtonian equations of motion (coupled ODE's) for particles in a discrete chain whose continuum limit is eq. (1.1). To avoid discreteness effects, we used chains of 600 particles and kink widths of 20 particles. In $K\overline{K}$ collisions, the kinks were started 300 particles (i.e., 15 kink widths) apart and, to save computer time, the spatial reflection symmetry $(x \rightarrow -x)$ of the system was used.

3. Kink–antikink scattering for $\eta < -\frac{1}{4}$

3.1. General considerations

In view of the potential applications to ^{3}He in the B phase [3–5], interactions of kinks and anti-kinks in the DSG model for $\eta < -\frac{1}{4}$ have been the subject of numerous previous studies [3–5, 27, 28, 35]. Among the important phenomena previously observed in collisions of kinks (with velocity v) with antikinks (with velocity $-v$) are (1) the trapping, at low velocity $(v < v_c \approx 0.359$ for $\eta =$

$-1.00)$, of a small $K\overline{K}$ pair to form a spatially localized, oscillatory (decaying "breather") final state; (2) the conversion, at very high velocity $(v \geq v_{con} \approx 0.92$ for $\eta = -1.00)$ [4], of a "small" $K\overline{K}$ pair to a "large" $K\overline{K}$ pair [28, 35]; and (3) the conversion, for essentially all velocities tested, of a "large" $K\overline{K}$ pair to a "small" $K\overline{K}$ pair [4, 28].

To complement and extend these prior results, we have focused our study on the scattering of "small" $K\overline{K}$ pairs at low velocities $(v \leq v_c)$ and for values of $\eta = -0.50$ and -1.00. From the form of the DSG potential for $\eta < -\frac{1}{4}$ (see fig. 1), the difference in energy between "small" and "large" kinks (cf. (2.2b) and (2.3b)), and elementary topological considerations, we expect that the interactions of these "small" $K\overline{K}$ pairs, for $v < v_{conv}$, will be similar to those in the ϕ^4 theory [30] in that the K and $\overline{K}$ can *not* pass through each other and thus will typically reflect. Further, given the existence of the shape mode around the small kinks, we expect that the "resonant energy exchange mechanism" developed in CSW and PC will apply and that there should exist considerable structure in these interactions, with ranges of initial velocity in which the $K\overline{K}$ are trapped alternating with ranges in which they escape after a second (or higher) interaction [30–31]. Indeed, our numerical results confirm these expectations quantitatively. Before presenting these results, let us recall in a minimally self-contained discussion the essential concepts and equations of the "resonant energy exchange mechanism"; readers interested in details and derivations are referred to CSW and PC. In picturesque physical terms, the central ideas are that in their interactions K and $\overline{K}$ can be viewed as particles which (1) have a mutually attractive potential [36], which can lead to trapping and (2) are individually deformable, with an internal oscillation corresponding to the "shape" mode discussed in section 2. During the first $K\overline{K}$ collision, these internal modes are excited, removing energy from the translational modes of the kinks and trapping them in their mutually attractive potential. Since the internal modes move with the kinks (essentially as adiabatic invariants) the energy

transferred to them is stored, not lost. Thus when the trapped kinks return for their second interaction (as they must, since they are trapped), this energy can be restored to the K and $\overline{K}$ translational motion, leading to escape for the K and $\overline{K}$, *if* an appropriate resonance condition is met. This condition has the form

$$\omega_s T_2 = 2 n_2 \pi + \delta_2, \tag{3.1}$$

where ω_s is the shape mode frequency, T_2 is the time between the first and second $\overline{KK}$ collision, δ_2 is an offset phase (between 0 and 2π by convention), and n_2 is an integer, which is the "order" of the resonance. Simple particle mechanics, applied to the individual kinks [30, 31], leads to the estimate for T_2 in terms of the $\overline{KK}$ binding energy, ε, (i.e., the amount by which the kinks are bound)

$$T_2 = \frac{\pi}{\omega_0(\eta)} \frac{1}{\sqrt{\varepsilon}}, \tag{3.2}$$

where $\omega_0(\eta)$ is the lowest frequency in the continuum (cf. (2.1)). This estimate is the leading term for $\varepsilon \to 0$. Heuristic arguments developed in CSW and PC, supported by empirical fits to the numerical data [30, 31], allow one to express the binding energy of the $\overline{KK}$ pair as a function of their initial velocity, v, in the center of mass; one finds [30, 31] for $v < v_c$, where v_c is the critical velocity for which the kinks first trap, that

$$\varepsilon(v) = \alpha(v_c^2 - v^2). \tag{3.3a}$$

Here the constant α is determined empirically from the data for $v > v_c$ according to [30, 31]

$$v_f^2 = \alpha(v^2 - v_c^2). \tag{3.3b}$$

Combining (3.2) and (3.3) leads an expression for T_2 in terms of v,

$$T_2(v) = \beta/(v_c^2 - v^2)^{1/2}, \tag{3.4a}$$

with

$$\beta = \pi/(\omega_0(\eta)\sqrt{\alpha}). \tag{3.4b}$$

Combining (3.4) with (3.1) leads to the prediction for those initial velocities, v_{n_2}, *below* the initial trapping velocity (v_c), which lead to resonant *escape* of the $\overline{KK}$ pair:

$$(v_c^2 - v_{n_2}^2) = \frac{\beta^2 \omega_s^2}{(2 n_2 \pi + \delta_2)^2}. \tag{3.5}$$

Thus the theory predicts a *sequence* of resonances, becoming increasingly dense as $v \to v_c$ from below. In addition, the width of the nth resonance is estimated [30] to fall (for large n) as $1/n^3$. Limitations on the range of n for which the theory is expected to apply are discussed in detail in CSW; in essence, one finds that n_2 cannot be too small (otherwise the leading order estimate for T_2 in (3.2) fails) nor too large (when T_2 becomes very long, the coupling through higher order nonlinear terms to nonlocalized modes which remove energy from the kink becomes important). Empirically, we shall find that in the DSG system for $\eta = -0.50$ resonances satisfying $3 \le n_2 \le 22$ can be observed.

3.2. "Small" $\overline{KK}$ scattering for $\eta = -0.50$

In fig. 4 we plot the DSG potential for $\eta = -0.50$, together with the "small" and "large" kink solutions. For this value of η, the continuum of small oscillations begins at $\omega_0 = 1/\sqrt{2} = 0.7071\ldots$ and the "shape" mode of the small kink occurs for $\omega = \omega_s = 0.6592\ldots$. Fig. 5 illustrates the potential for linear oscillations around the "small" kink, V_{SCH}^{I}, (fig. 5a), and the spatial distribution of the wavefunction of the shape mode (fig. 5b); for completeness, the potential for linear oscillations around the large kink, V_{SCH}^{II}, for which there is no shape mode, is also shown (fig. 5c).

Using the analytic forms of the "small" K and $\overline{K}$ solutions (see eq. (2.2)) for $\eta = -0.50$ as initial conditions [37] we have studied $\overline{KK}$ scattering in the velocity range $0.20 \le v \le 0.40$. In fig. 6 we plot
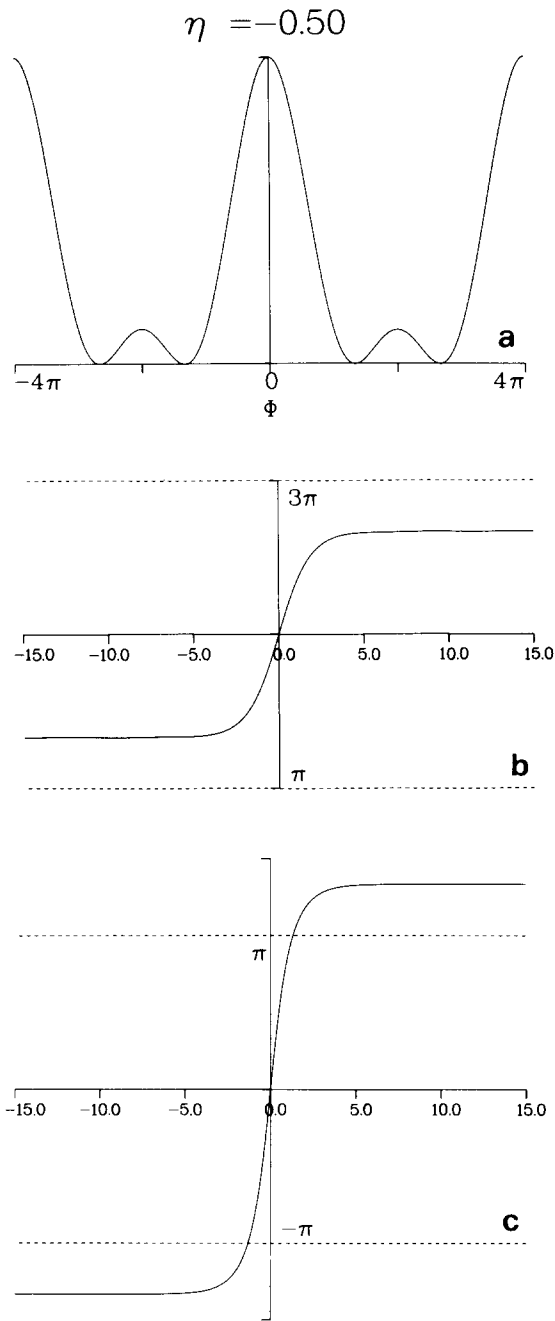
$\eta = -0.50$

$\eta = -0.50$

Fig. 4. A plot for $\eta = -0.50$ of a) the DSG potential; b) the "small" kink solution; and c) the "large" kink solution.
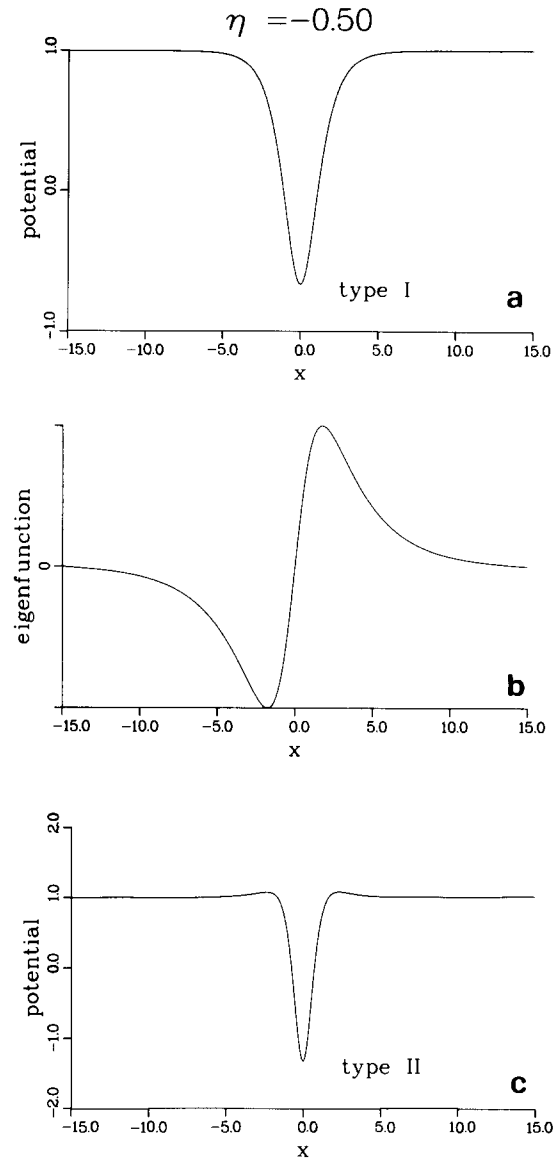
Fig. 5. a) The potential, $V^{I}_{\text{SCH}}(x) \equiv d^2 V(\phi)/d\phi^2 |_{\phi_K}$, determining the linear oscillations around the "small" kink for $\eta = -0.50$; b) the spatial distribution of eigenfunction corresponding to the localized, "shape" mode of the "small" kink. Note that, as expected, this mode corresponds to the first excited state in this potential, since the ground state is the translation (Goldstone) mode of the kink; c) the potential, $V^{II}_{\text{SCH}}(x) \equiv d^2 V(\phi)/d\phi^2 |_{\phi_K}$, determining the linear oscillations around the "large" kink for $\eta = -0.50$. The only localized mode in this potential in the translation (Goldstone) mode; there is *no* localized shape oscillation of the large kink.
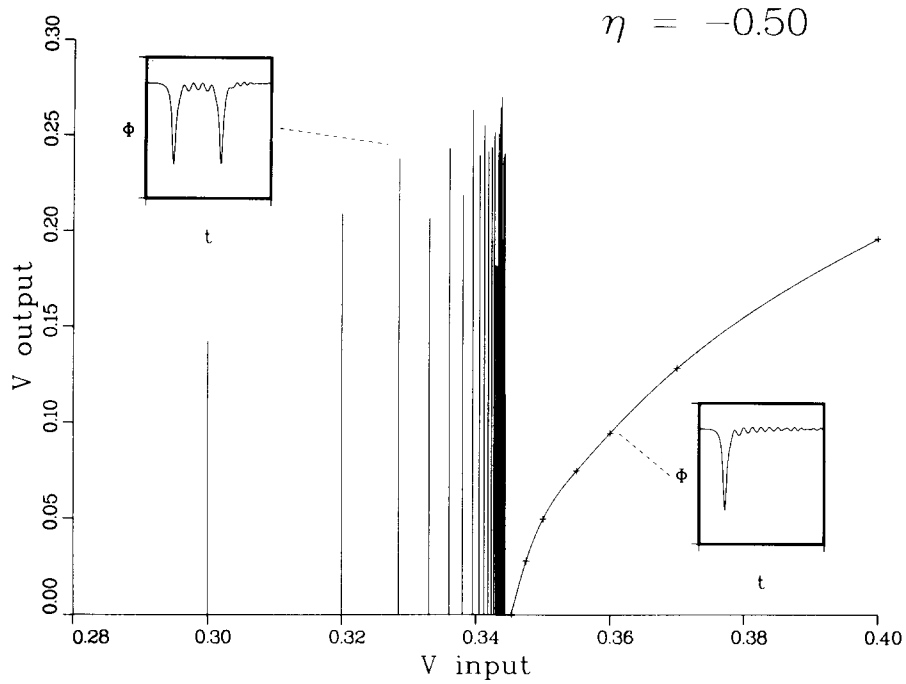
$$\eta = -0.50$$

Fig. 6. The outgoing velocities (V output) of the "small" DSG kink and antikink as a function of their incoming velocities (V input) for $\eta = -0.50$. The vertical lines below $v = v_c = 0.345\ldots$ indicate the resonances in which the K and $\overline{\text{K}}$ reappear in the final state. Note that the widths of these resonances are *not* depicted on this figure. The nature of the $\text{K}\overline{\text{K}}$ collision is indicated by the insets, which show $\phi(x = 0, t)$ versus t.

Table I
Analysis of two-bounce windows in "small" $\text{K}\overline{\text{K}}$ scattering for $\eta = -0.50$

Position of resonance v_{n_2}	Final velocity v_f	Time between first and second interactions T_2	$\beta = T_2(v_c^2 - v_{n_2}^2)^{1/2}$	$\omega_s T_2/2\pi$	Index n_2	Theoretical value of v_{n_2}
0.3000	0.1425	35.63	6.092	3.731	3	0.30446
0.3200	0.2094	43.41	5.633	4.555	4	0.32047
0.3285	0.2385	53.03	5.642	5.564	5	0.32857
0.3330	0.2075	62.29	5.689	6.536	6	0.33324
0.3360	0.2436	72.12	5.741	7.567	7	0.33620
0.3380	0.2192	82.23	5.808	8.628	8	0.33818
0.3395	0.2643	92.91	5.855	9.748	9	0.33958
0.3405	0.2403	103.02	5.911	10.809	10	0.34060
0.3412	0.2557	112.07	5.946	11.7588	11	0.34137
0.3418	0.2420	121.76	5.971	12.775	12	0.34197
0.3423	0.2442	131.52	5.972	13.799	13	0.34244
0.3427	0.2523	140.99	5.963	14.793	14	0.34281
0.3430	0.1824	149.69	5.956	15.705	15	0.34312
0.34330	0.2517	159.80	5.930	16.7665	16	0.34337
0.34355	0.2649	169.74	5.893	17.808	17	0.34358
0.34375	0.2708	179.46	5.865	18.828	18	0.34376
0.34395	0.1954	190.35	5.806	19.971	19	0.34391
0.34410	0.2392	198.126	5.698	20.786	20	0.34405
0.34425	0.2411	209.376	5.634	21.967	21	0.34416
0.34435	0.1145	217.22	5.560	22.790	22	0.34425

Table II
Width of the resonances for $\eta = -0.50$ for several values of n_2

Index, n_2	Observed width in velocity, Δv	Product, $X = (n_2 + \delta_2/2\pi)^3 \cdot \Delta v$
5	$(1.90 \pm 0.1) \times 10^{-3}$	0.360 ± 0.020
9	$(0.40 \pm 0.1) \times 10^{-3}$	0.370 ± 0.090
14	$(1.14 \pm 0.1) \times 10^{-4}$	0.365 ± 0.003
17	$(6.95 \pm 0.15) \times 10^{-5}$	0.388 ± 0.009

the outgoing velocity of the kinks as a function of their incoming velocity. For $v > v_c = 0.3453\ldots$ we see that, as anticipated, the K and $\overline{\text{K}}$ reflect; this is indicated by the right inset of fig. 6, which shows that $\phi(x = 0, t)$ for $v > v_c$ returns to its initial value $(= 2\cos^{-1}(1/4\eta))$ at large time. For $v < v_c$, we see in fig. 6 the expected resonances; as shown by the left inset, these are indeed "two-bounce" resonances. In table I we present the results of applying the "resonant energy exchange" theory [30, 31] summarized above to these numerical data. Altogether, twenty resonances ($n = 3$ to $n = 22$) were observed, and the fit to the theoretical predic-

tions is excellent. Several specific remarks are in order. First, the values of β and δ_2 used to determine the theoretical velocities, v_{n_2}, at the centers of the resonances were deduced from the mean values of the observed quantities $T_2 \times (v_c^2 - v^2)^{1/2}$ and $(\omega_s T_2 - 2n_2\pi)$ and were found to be $\beta = 5.815\ldots$ and $\delta_2/2\pi = 0.745\ldots$. Although δ_2 is a parameter which the theory cannot predict, since it depends on the details of the K$\overline{\text{K}}$ interaction at short range, β, as shown by (3.4b), should be given by $\beta = \pi\sqrt{2}/\sqrt{\alpha} = 5.990$, since our fits to the data for $v > v_c$ give $\alpha = 0.55$. This 3% agreement between "predicted" and "observed" values of β is consistent with the level of accuracy found in previous applications of the resonant energy exchange mechanism [30, 31]. Second, the observed variation in the final velocity, v_f, of the resonances (compare $n = 15$ to $n = 14$ and 16, for example) arises, as in our previous studies [30, 31], from the fact that for most resonances we did not attempt to scan through the resonance carefully to determine the maximum outgoing velocity corre-
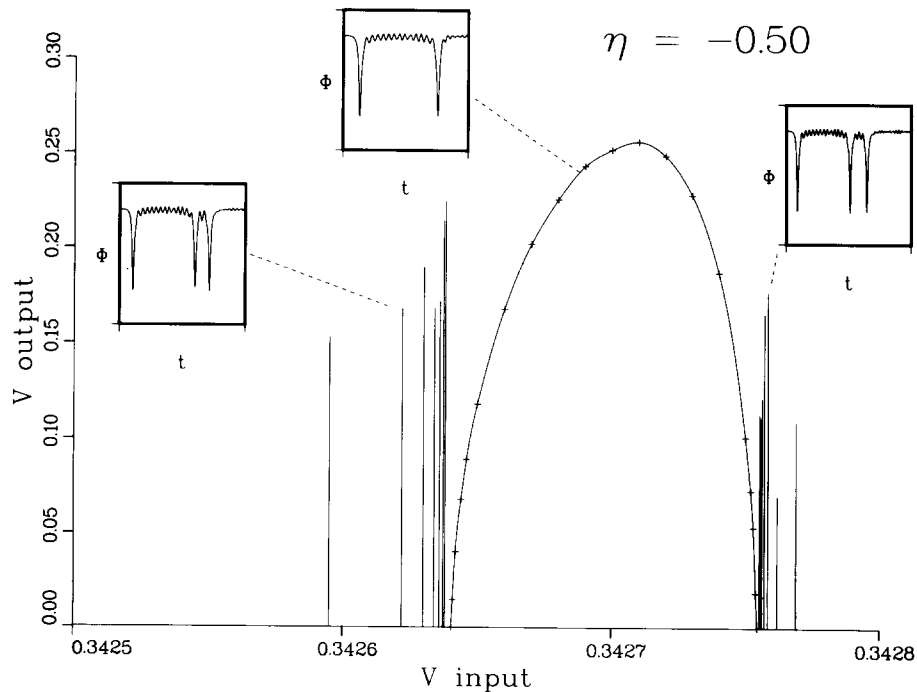

Fig. 7. The outgoing velocities (V output) versus the incoming velocities (V input) for the three-bounce resonances (vertical lines) observed near the edges of the $n_2 = 14$ two-bounce resonance for $\eta = -0.50$. The insets show the behavior of $\phi(x = 0, t)$.

sponding to a given resonance. That this output velocity is extremely sensitive to the precise input velocity is clear in principle from the theory and will be demonstrated in great detail shortly. Third, in CSW we argued that the width of the resonances in initial velocity, Δv, should be proportional to $(2n_2\pi + \delta_2)^{-3}$, so that the resonances rapidly become extremely narrow as n_2 increases. In table II we exhibit the width of four of the observed resonances, covering the range from $n_2 = 5$ to $n_2 = 17$. The constancy of the product $\Delta v \times (2n_2\pi + \delta_2)^3$ is satisfied to 5%.

All in all, our numerical results for the "two-bounce" resonances in the DSG model for $\eta = -0.50$ provide a striking confirmation of the resonant energy exchange mechanism. In view of its previous successes in similar models [30, 31], however, this is perhaps not surprising. It may therefore be of greater interest to discuss the higher bounce resonances, which we have studied quantitatively for the first time in this model. In fig. 7 we show (on a greatly expanded horizontal scale) a plot of initial velocities in the region of the $n = 14$ two-bounce resonance. Apart from providing a very accurate determination of the resonance width and illustrating the dramatic sensitivity of the output velocity to the exact input velocity within a resonance, our data show clearly sequences of *three*-bounce resonances – see insets – on *both* sides of the two-bounce resonance. Before discussing these data in detail, we note that we have observed this phenomenon around other two-bounce resonances; fig. 8 shows three-bounce resonances *below* the $n = 17$ two-bounce resonance [38]. Further, and, very interestingly, the answer to the obvious question – "Does this structure of resonances upon resonances continue?" – is "yes". In fig. 9 we illustrate a sequence of *four*-bounce resonances just below the lowest *three*-bounce resonance shown in fig. 7. In addition, individual *five*-bounce resonances have been seen (see, for example, the lowest resonance in fig. 8).

The detailed numerical results on the three-bounce resonances around the $n = 14$ two-bounce resonance are presented in tables III and IV. From

fig. 7 and these tables several important features of these resonances are immediately clear:

1) the three-bounce resonances occur at the edge of two-bounce resonances;

2) the sequences of three-bounce resonances show structure very similar to that seen in the two-bounce resonances, with three-bounce resonances accumulating as one moves to the threshold at the edge of the two-bounce resonance;

3) the small oscillations in data on $\phi(0, t)$, shown on the insets of fig. 8, suggest that the sequence of three-bounce resonances corresponds to a series of resonant interactions *with the same frequency*, ω_s, that occurs in the two-bounce resonances; that is, the three-bounce resonances seem to be determined by an equation of the form

$$\omega_s T_3 = 2\pi n_3 + \delta_3, \tag{3.6}$$

where T_3 is the time between the second and third collision, δ_3 is a phase shift ($0 < \delta_3 < 2\pi$) and n_3 is an integer; and

4) the shape of the two-bounce resonance, as shown in fig. 7, is asymmetric, with the large v side ($v \lesssim v_{c''}$) being much steeper than the small v side ($v \gtrsim v_{c'}$); correspondingly, the spacing of the three-bounce resonances *above* $v_{c''}$ is much closer than that of those *below* $v_{c'}$.

The first two features provide a strong qualitative hint that the resonant energy exchange mechanism is operating, whereas the last two give semi-quantitative hints as well. In particular, the relation between the steepness of the outgoing velocity and the spacing of the resonances is just what one would expect from the arguments presented in CSW and PC. Consider fitting the outgoing velocity within the two-bounce resonance window by a formula analogous to (3.3b)

$$v_f^2 = \alpha' |v_{c'}^2 - v^2|. \tag{3.7}$$

This fit amounts to an expansion around the lower critical velocity, $v_{c'}$. Clearly, one could make a similar fit around the upper critical velocity, $v_{c''}$, with a different coefficient, α''. From fig. 7, $\alpha'' > \alpha'$.
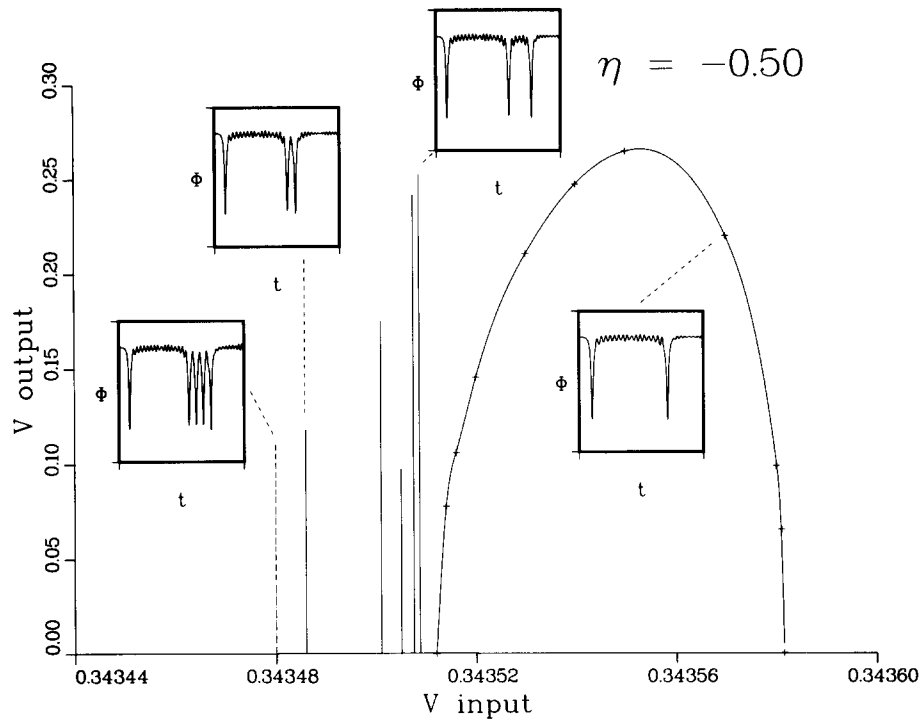
Fig. 8. The outgoing velocities (V output) versus the incoming velocities (V input) for the three-bounce resonances (solid vertical lines) observed below the $n_2 = 17$ two-bounce resonance for $\eta = -0.50$. Comparison of the two upper most insets shows the characteristic differences between the number of shape mode oscillations for three-bounce resonances of different index, n_3. The dotted vertical line (at $V_{input} = 0.34348$) represents an observed five-bounce resonance.
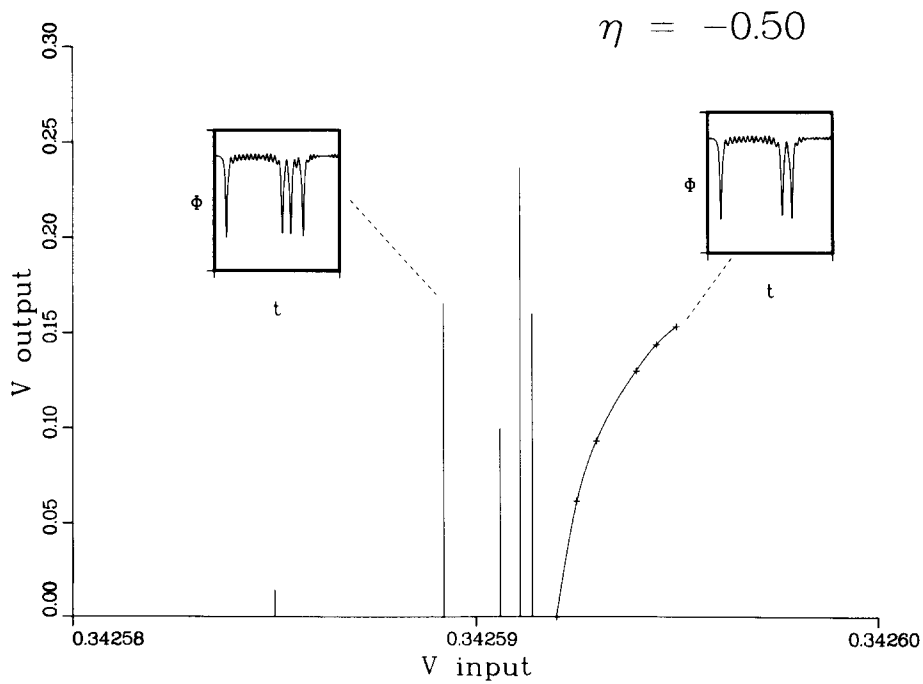

Fig. 9. The outgoing velocities (V output) versus the incoming velocities (V input) for the four-bounce resonances observed below the $n_3 = 2$, $n_2 = 14$_ resonance.

Table III

Three-bounce resonances observed just *below* the minimum velocity for the $n_2 = 14$ two bounce resonance; $v_{c'} = v_c(14_-) = 0.3426405(5)$

Position of resonance v_{n_3}	Final velocity v_f	Time between second and third interactions T_3	$\beta =$ $T_3(v_c^2 - v_n^2)$	$\omega_s T_3/2\pi$	Index n_3	Theoretical value of v_{n_3}
0.342595	0.1533	21.34	11.97×10^{-2}	2.240	2	0.3425940
0.342622	0.1684	32.202	11.62×10^{-2}	3.378	3	0.3426194
0.342630	0.1898	41.51	11.40×10^{-2}	4.355	4	0.3426286
0.342634	0.1685	51.51	11.28×10^{-2}	5.403	5	0.3426330
0.342636	0.1721	60.74	11.25×10^{-2}	6.373	6	0.3426354
0.3426374	0.2146	71.81	11.28×10^{-2}	7.534	7	0.3426368
0.3426381	0.2248	80.64	11.40×10^{-2}	8.460	8	0.3426378

Table IV

Three-bounce resonances observed just *above* the maximum velocity for the $n_2 = 14$ two bounce resonance; $v_{c''} = v_c(14_+) = 0.3427545(5)$

Position of resonance v_{n_3}	Final velocity v_f	Time between second and third interactions T_3	$\beta'' =$ $T_3(v_{c''}^2 - v_{n_3}^2)^{1/2}$	$\omega_s T_3/2\pi$	Index n_3	Theoretical value of v_{n_3}
0.3427690	0.1092	24.88	7.95×10^{-2}	2.610	2	0.34276789
0.3427620	0.0701	34.062	7.93×10^{-2}	3.574	3	0.34276145
0.3427585	0.1771	45.43	7.89×10^{-2}	4.768	4	0.34275865
0.3427572	0.1660	54.32	7.92×10^{-2}	5.699	5	0.34275719
0.3427563	0.1218	64.55	7.93×10^{-2}	6.773	6	0.34275634
0.3427558	0.1111	73.34	7.92×10^{-2}	7.695	7	0.34275579
0.3427554	0.1130	83.86	7.92×10^{-2}	8.798	8	0.34275543

If one now applies the standard resonant energy exchange analysis, one obtains for the locations of the three bounce resonances, v_{n_3}, located *below* $v_{c'}$, the equations

$$|v_{c'}^2 - v_{n_3}|^2 = \frac{\pi^2 \omega_s^2}{\omega_0(\eta)^2 \alpha'(2n_3\pi + \delta_3)^2}. \qquad (3.8)$$

A similar equation will apply to resonances *above* $v_{c''}$. Since $\alpha'' > \alpha'$, one expects the resonances on the high side to be more closely grouped around $v_{c''}$ than those on the low side are around $v_{c'}$; this is precisely what is observed.

Buoyed by this semi-quantitative consistency, we have applied the standard formulae of the resonant energy exchange mechanism to the three bounce resonances. The results are in remarkable quantitative agreement with the theory. In particu-

lar, the products $\beta' \equiv T_3 \times (v_{c'}^2 - v^2)^{1/2}$ and $\beta'' = T_3 \times (v^2 - v_{c''}^2)^{1/2}$ are, as anticipated by the theory, constant to high accuracy (5% for β', 1% for β'', see tables III and IV). The values of δ_3, although less well determined, are also reasonably constant ($\delta_3' = \pm 25\%$ and $\delta_3'' = \pm 20\%$). Clearly the resonant energy exchange mechanism is at work. Indeed, as in PC, we were able to observe the large number of three bounce resonances only because, on the basis of the formula, we were able to predict their locations.

There are two important questions that should be answered before a true quantitative picture can be claimed, however. First, why do the observed three-bounce resonances occur at the edge of two-bounce resonances (and similarly, from fig. 9, four-bounce resonances at the edge of three-bounce resonances)? Second, can the theory predict the

large difference in scale between $\beta \equiv T_2 \times (v_c^2 - v_n^2)^{1/2}$ shown in table I and β' or β''?

To answer these questions, we need to extend the detailed analysis of two-bounce scattering developed in CSW to the three (and higher) bounce case. Since the full motivations and derivations are available in CSW, we shall simply sketch the arguments here.

Let S be the (complex) amplitude of the shape mode at time $t = 0$, so that the full space and time variation of this mode is

$$\Psi_s(x, t) = (S e^{i\omega_s t} + S^* e^{-i\omega_s t})\psi_s(x), \qquad (3.9)$$

where $\psi_s(x)$ is the spatial wavefunction (as shown, for example, in fig. 5b) for the mode. For a given S, the total energy in the shape mode of a single kink is

$$E_s = 2|S|^2 \omega_s^2. \qquad (3.10)$$

$K\overline{K}$ collisions can excite (or de-excite) the shape modes. A useful visualization of the sequence of two-, three-, ... bounce interactions is presented in fig. 10. Here the locations of the centers of the K and $\overline{K}$ are plotted versus time for interactions in which the K and $\overline{K}$ emerge with the final state after 1, 2, 3, 4, and 5 collisions. In CSW, we assumed that the shape mode immediately *after* a collision, S', was related to that immediately *before*, S, by the simple linear relation [39]

$$S' = aS + bS^* + \rho, \qquad (3.11)$$

and then showed that general constraints (eg., time reversal invariance) implied relations among a, b, and ρ such that

$$S' = \frac{-\rho}{\rho^*}(1 + i\gamma)S + i\gamma S^* + \rho, \qquad (3.12)$$

where γ is purely real. In principle, both γ and ρ are expected to vary with v, but only rather slowly. Since the resonances occur in a relatively narrow range of velocities near v_c, we neglect this dependence here. From (3.12), the general condition for
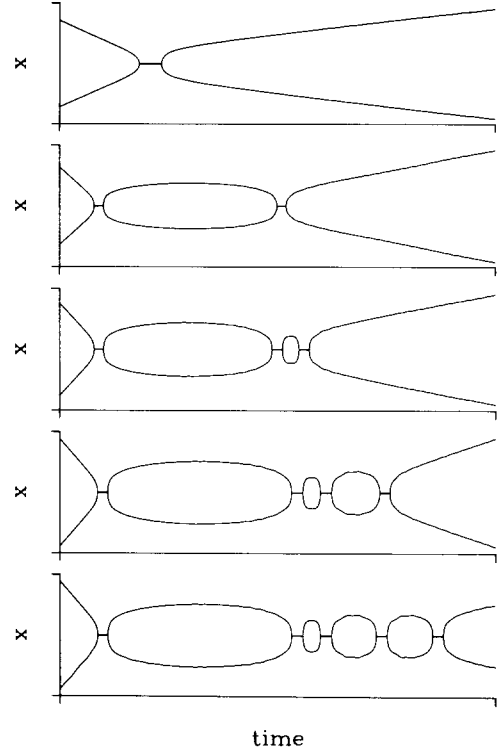

Fig. 10. Plots for the locations of the kink and antikink versus time for several different sequences of interactions leading finally to escape of the K and $\overline{K}$. From the top down, these interactions involve, respectively, 1, 2, 3, 4, and 5 $K\overline{K}$ collisions.

resonance after two interactions can be derived. In addition, one can derive an expression for the width of the resonances. In the ϕ^4 simulation – and, as we shall see later, for the DSG as well – the resonance width was consistent with $\gamma \approx 0$. Taking this hint, let us study the three-bounce resonance condition when $\gamma = 0$ in (3.12).

Immediately *after* the first $K\overline{K}$ collision, which we shall take as defining $t = 0$, (3.12) (with $\gamma = 0$) shows that $S' = \rho$. Just before the second collision occurs, at $t \equiv T_2$, this S'' has evolved to $S'(T_2) = \rho\, e^{i\omega_s T_2}$, so that immediately *after* the second collision, one has

$$S'' = -\rho/\rho^*(\rho\, e^{i\omega_s T_2}) + \rho \qquad (3.13a)$$

$$= \rho[1 - e^{i(2\theta + \omega_s T_2)}], \qquad (3.13b)$$

where we have introduced $\theta \equiv \arg \rho$. Note that the resonance condition for the two bounce collision is particularly transparent in this $\gamma = 0$ case. From (3.13b), to have *no* energy in the shape mode ($|S''| = 0$) so that the kinks are most likely to escape, one needs

$$\omega_s T_2 + 2\theta = 2n_2\pi, \qquad (3.14)$$

exactly the familiar condition (3.1) with $\delta_2 \equiv 2\theta$. In CSW we presented arguments that the width of the resonances should be constant in the phase, $\chi \equiv \omega_s T_2 + 2\theta - 2n_2\pi$. Note that $\chi = 0$ exactly on resonance. The value of $\chi \equiv \chi_0$ at which the resonance disappears should be determined by the condition that the energy in the shape mode after the second collision be precisely equal to what it was before: that is, using (3.13b) and (3.10),

$$2\omega_s^2|\rho|^2|1 - e^{i\chi_0}|^2 = 2\omega_s^2|\rho|^2 \qquad (3.15a)$$

so that

$$\cos\chi_0 = \tfrac{1}{2} \qquad (3.15b)$$

and thus

$$\chi_0 = \pm\pi/3. \qquad (3.15c)$$

Thus (3.15c) implies that the two-bounce resonances should disappear at values of $T_2^{(\pm)}$ defined by

$$\omega_s T_2^{(\pm)} + 2\theta - 2n_2\pi = \pm\pi/3. \qquad (3.16)$$

Now consider the third $K\overline{K}$ collision, which occurs at time T_3 *after* the second collision. The amplitude, S'', immediately before the third collision is thus $S'' = \rho[1 - e^{i(2\theta + \omega_s T_2)}]e^{i\omega_s T_3}$, so (3.12), with $\gamma = 0$, gives the amplitude (S''') immediately *after* the third collision as

$$S''' = -e^{2i\theta}\left[\rho(1 - e^{i(2\theta + \omega_s T_2)})\right]e^{i\omega_s T_3} + \rho$$

$$= \rho[1 - e^{i(2\theta + \omega_s T_3)} + e^{i(4\theta + \omega_s(T_2 + T_3))}]. \qquad (3.17)$$

Thus the resonance condition $|S'''| = 0$ can be written as

$$1 + e^{i\nu_1} + e^{i\nu_2} = 0 \qquad (3.18)$$

with $\nu_1 = 2\theta + \omega_s T_3 + \pi$ and $\nu_2 = 4\theta + \omega_s(T_2 + T_3)$ which has the solutions

$$\nu_1 = 2\pi/3 + (2m_1\pi) \qquad (3.19a)$$

and

$$\nu_2 = -2\pi/3 + (2m_2\pi) \qquad (3.19b)$$

or $\nu_1 \rightleftharpoons \nu_2$; here m_1 and m_2 are arbitrary integers. In terms of T_2 and T_3, we see that the resonance conditions become *either*

$$\omega_s T_3 + 2\theta = -\pi/3 + 2m_1\pi \qquad (3.20a)$$

and

$$\omega_s T_2 + 2\theta = -\pi/3 + 2(m_2 - m_1), \qquad (3.20b)$$

or

$$\omega_s T_3 + 2\theta = +\pi/3 + 2m_1'\pi \qquad (3.21a)$$

and

$$\omega_s T_2 + 2\theta = +\pi/3 + 2(m_2' - m_1')\pi. \qquad (3.21b)$$

Note that eq. (3.20b) and (3.21b) are *exactly* the conditions, (3.16), determining the *edges* of the two-bounce resonances. Hence we *predict* that the three-bounce resonances should occur at the edge of two-bounce resonances, exactly as our data indicate. A similar analysis for the case of four $K\overline{K}$ collisions shows that four-bounce resonances should occur, as observed, at the edge of three-bounce resonances.

Turning to the second of the questions posed above, we ask whether our approach can account for the large difference between $\beta \equiv T_2 \times (v_c^2 - v^2)^{1/2}$ and $\beta' \equiv T_3 \times (v_c^2 - v^2)^{1/2}$ and $\beta'' \equiv T_3 \times (v^2 - v_{c'}^2)^{1/2}$. To study this point let us focus on β', that is, on the three-bounce resonances just below $v_{c'}$. First, as indicated by (3.3), the value of

β' should be related to α' in (3.7) according to (see (3.4b)) $\beta' = \pi/(\omega_0(\eta)(\alpha')^{1/2})$. Using the "experimental" fit to α' ($\approx 2.3 \times 10^{+3}$), we find $\beta' = 9.9 \times 10^{-2}$, which is 15% agreement with the observed value shown in table III. This level of agreement is consistent with previous results in other models [30, 31]. Second, one can make a much more demanding test of the theory by trying to *predict* the magnitude of α' and hence β' from previously known parameters. This is possible since our analysis essentially determines the dependence of the shape mode energy as a function of time between collisions (and therefore as a function of initial velocity) for the whole region near v_c. Explicitly, we note that for two-bounce resonance window region, $v_{c'} < v < v_{c''}$, total energy conservation can be written

$$Mv_f^2 = -E_s(v^2) + E_s(v_{c'}^2)$$

$$\approx -\frac{\partial E_s}{\partial v^2}\bigg|_{v_{c'}} (v^2 - v_{c'}^2) + \cdots . \quad (3.22)$$

From (3.10) and (3.17), we know that

$$E_s(v) = 8|\rho|^2\omega_s^2[1 - \cos(\omega_s T_2(v) + 2\theta_0)]. \quad (3.23)$$

Since we have always assumed ρ to be weakly dependent on v, the only v dependence comes from $T_2(v)$ and is explicitly given in (3.4). Working through the algebra and using $8|\rho|^2\omega_s^2 = 2Mv_c^2$ and $\sin(\omega_s T_2(v_{c'}) + 2\theta_0) = \sqrt{3}/2$ (from (3.15)), we

obtain

$$v_f^2 = \left(v_c^2 \frac{\sqrt{3}}{2}\omega\beta\right)/(v_c^2 - v_{c'}^2)^{3/2}(v^2 - v_{c'}^2), \quad (3.24)$$

which, comparing to (3.7), amounts to a prediction of α'. Plugging in the approximate values, we obtain $\alpha' = 5.06 \times 10^3$; although off by a factor of 2 from the experimental α' ($= 2.3 \times 10^3$), this does give the correct order of magnitude and amounts to an a priori prediction of the two-order-of-magnitude difference between β and β'.

The same analysis can be applied to the region near the upper critical velocity ($v_{c''}$) of the two bounce window. We find similar rough agreement and predict the asymmetry $\alpha'' > \alpha'$, although not to the extent observed in the data. It appears that a full quantitative explanation of these results requires a more detailed modelling of the $K\overline{K}$ interactions.

One can extend the analysis presented here to higher bounce resonances. In particular, one finds that four-bounce resonances should occur at the edges of the three-bounce windows and that a formula analogous to (3.8) correctly predicts their locations. In table V we present data on the four-bounce resonance observed just below the $n_2 = 14$, $n_3 = 1$, three-bounce resonance (fig. 8); the agreement between the theoretical and observed values of the resonances is again quite good.

It is natural to wonder whether this "resonance upon resonance" structure continues, in a manner reminiscent of the self-similar/structures-on-all-

Table V

Four-bounce resonances observed just *below* the minimum velocity for the $n_2 = 14 n_3 = 1$ three-bounce resonance, $v_{c'''} = v_c(14_-, 1_-) = 0.3425921(2)$

Position of resonance v_4	Final velocity v_f	Time between third and fourth interactions, T_4	$\beta''' = T_3(v_{c'''}^2 - v_{n_4}^2)^{1/2}$	$\omega_s T_4/2\pi$	Index n_4	Theoretical value of v_{n_4}
0.3425850	0.0144	20.51	4.37×10^{-2}	2.152	2	0.34258657
0.3425892	0.1652	30.84	4.35×10^{-2}	3.236	3	0.34258940
0.3425906	0.0997	42.02	4.26×10^{-2}	4.408	4	0.34259051
0.3425911	0.2367	50.99	4.22×10^{-2}	5.350	5	0.34259106
0.3425914	0.1602	61.08	4.23×10^{-2}	6.408	6	0.34259136

scales behavior observed in certain chaotic dynamical systems. With our present numerical precision [37], at a level between the four- and five-bounce resonances the width of the windows in V_{init} approaches the size of discreteness effects on the (nominal) kink velocities, and we then cannot make accurate determinations beyond this order. More fundamentally, since our "resonant energy exchange mechanism" ignores the (effectively "inelastic") coupling to non-localized small oscillations, the fine structure of the very high-order resonances must be blurred even in an arbitrarily precise numerical simulation. Obtaining an analytic estimate for the limits to the "resonance upon resonance" structure remains an interesting open problem.

3.3. "Small" $K\bar{K}$ scattering for $\eta = -1.00$

In view of both the experimental interest [3–5] and previous numerical studies [27–28] in the case $\eta = -1.00$, we present here results of a detailed analysis of the two-bounce resonances for this value. The structure is very similar to that observed for $\eta = -0.50$, except that the resonances are somewhat narrower and therefore more difficult to find.

In fig. 3 we show the DSG potential for $\eta = -1.00$, together with the "small" and "large" kink solutions. For this value of η, the continuum of small oscillations begins at $\omega_0 = \sqrt{3}/2 = 0.8660\ldots$ and the shape mode of the small kink occurs at $\omega = \omega_s = 0.8409\ldots$. In fig. 11 we display the potential for linear oscillations around the small kink, V^{II}_{SCH}, the spatial structure of the wavefunction for the shape mode, and finally the potential for linear oscillations around the large kink, V^{I}_{SCH}, for which there is no shape mode.

We have studied numerically $K\bar{K}$ interactions – using the analytic forms of the K and $\bar{K}$ for $\eta = -1.00$ as initial conditions – in the velocity range $0.25 \leq v \leq 0.40$. In fig. 12 we plot the outgoing velocity of the kink as a function of the incoming velocity. For $v \geq v_c \approx 0.35907\ldots$ the K and $\bar{K}$ reflect, as indicated by the rightmost inset
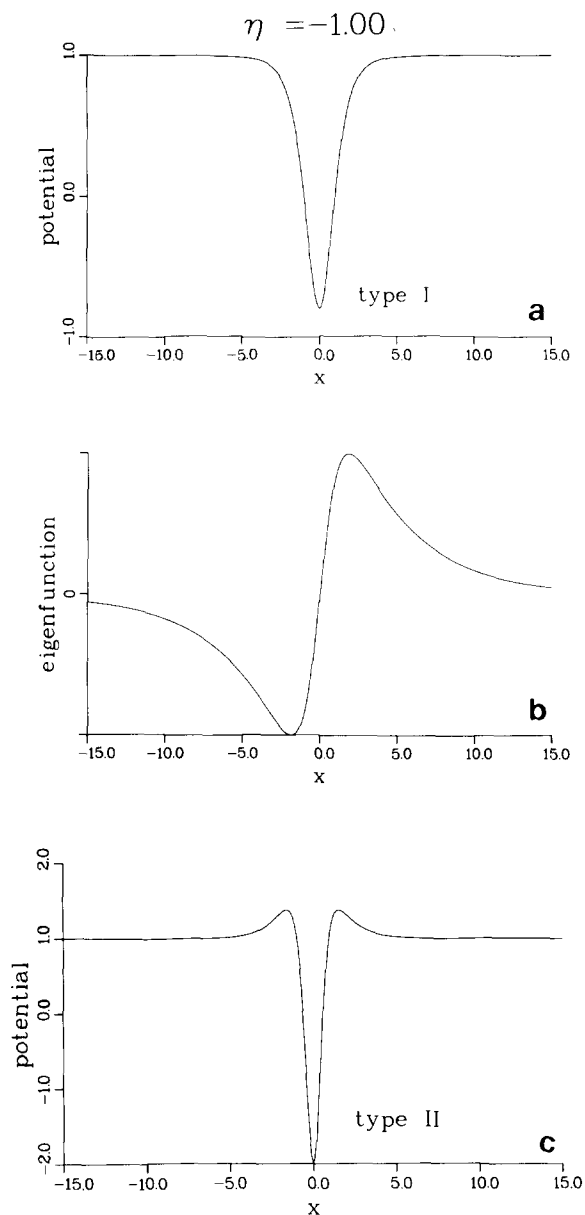
$\eta = -1.00$

Fig. 11. a) The potential, $V^{I}_{SCH}(x) \equiv dV(\phi)/d\phi|_{\phi_K^I}$, determining the linear oscillations around the "small" kink for $\eta = -1.00$; b) the spatial distribution of the eigenfunction corresponding to the "shape" mode of the "small" kink. As in fig. 5, this mode corresponds to the first excited state in this potential. Note that this $\eta = -1.00$ shape mode is slightly less localized than the same mode for $\eta = -0.50$; c) the potential, $V^{II}_{SCH}(x) \equiv d^2V(\phi)/d\phi^2|_{\phi_K^{II}}$, determining the linear oscillations around the "large" kink for $\eta = -1.00$. As in fig. 5, the only localized mode in this potential is the translation (Goldstone) mode; there is no localized shape oscillation of the large kink.
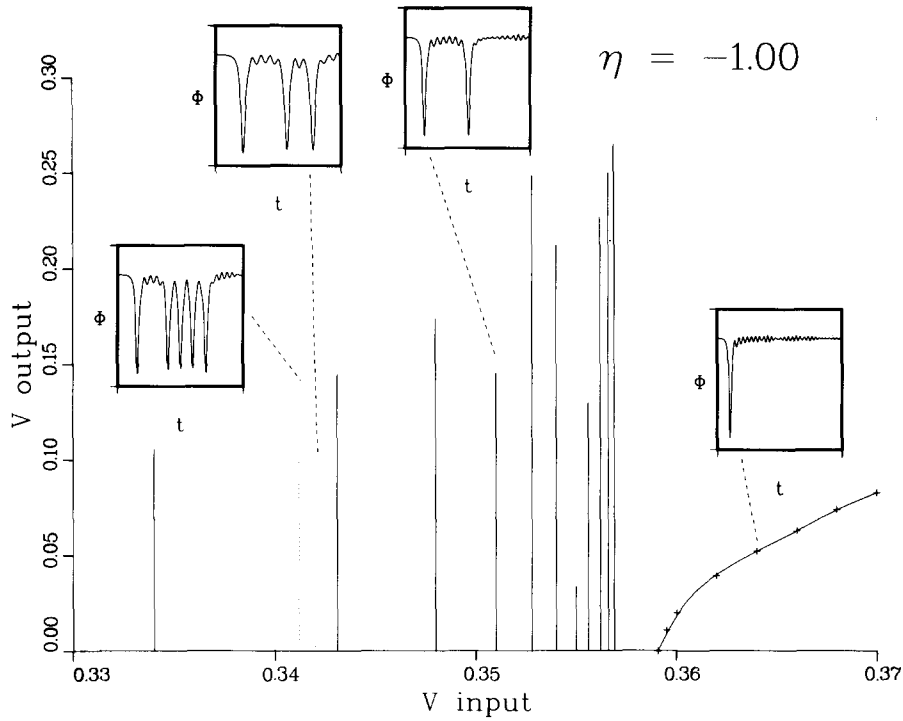
Fig. 12. The outgoing velocities (V output) of the small DSG kink and antikink as a function of their incoming velocities (V input) for $\eta = -1.00$. The vertical lines below $v = v_c \approx 0.359\ldots$ indicate the resonances in which the K and $\overline{\text{K}}$ appear in the final state. Note that the widths of the resonances are not depicted on this figure. The nature of the $\overline{\text{KK}}$ collision is indicated by the insets, which show $\phi(0, t)$ versus t.

Table VI

Analysis of two-bounce windows in "small" $\overline{\text{KK}}$ scattering for $\eta = -1$

Position of reso- nance v_n	Final velocity v_f	Time be- tween the 2 first bounce T_2	$\beta = T_2(v_c^2 - v_n^2)^{1/2}$	$\omega_s T_2/2\pi$	Index n	Theoretical v_n
0.3340	0.1059	32.96	4.345	4.513	4	0.33652
0.3431	0.1449	40.30	4.268	5.518	5	0.34397
0.3480	0.1739	47.81	4.230	6.546	6	0.34825
0.3510	0.1452	55.72	4.218	7.629	7	0.35093
0.3528	0.2491	63.00	4.209	8.627	8	0.35272
0.3540	0.2124	70.17	4.219	9.609	9	0.35398
0.3550	0.0340	78.45	4.229	10.742	10	0.35490
0.3556	0.1297	84.95	4.230	11.631	11	0.35559
0.3562	0.2273	93.29	4.227	12.774	12	0.35612
0.3566	0.2505	100.69	4.233	13.787	13	0.35654
0.3569	0.2655	107.57	4.239	14.723	14	0.35687

to fig. 12. For $v < v_c$, we see the expected series of two-bounce resonances; the fit of the "resonant energy exchange" theory to these data is summarized in table VI. As in the previous case ($\eta = -0.50$), the comparison of "experimentally" determined $\beta_{exp} = 4.24\dots$ with the "theoretically" predicted $\beta_{theor} = 4.04\dots$ is quite good. As usual, knowledge of the theoretical values of v_n was essential in finding the higher-lying, narrower resonances. We find $\delta_2/2\pi = 0.6365\dots$.

In addition to the two-bounce resonances, fig. 12 illustrates isolated "three-bounce" and "five-bounce" resonances. We did not study these features systematically, but considering the success of the multi-bounce theory for $\eta = 0.50$, we feel confident that these resonances also arise from resonant energy exchange.

4. Kink–antikink scattering for $-\frac{1}{4} < \eta < 0$

In the region $-\frac{1}{4} < \eta < 0$, the DSG potential is topologically similar to the sine-Gordon model, and there exists a single type of kink solution with the form given by eq. (2.4). In figs. 13a and 13b we plot the forms of the DSG potential and the kink solution for two values of $\eta(-0.05$ and $-0.15)$ in this region. Importantly, as illustrated in fig. 2, for $-\frac{1}{4} < \eta < 0$ there is *no* "shape" mode in the small oscillations around the kink. Thus, on the basis of the theory developed in CSW and successfully tested on a model *without* a shape mode in PC, we expect that there will be *no* resonances in $K\overline{K}$ scattering here.

We have studied extensively $K\overline{K}$ collisions for both $\eta = -0.05$ and $\eta = -0.15$. Below the critical

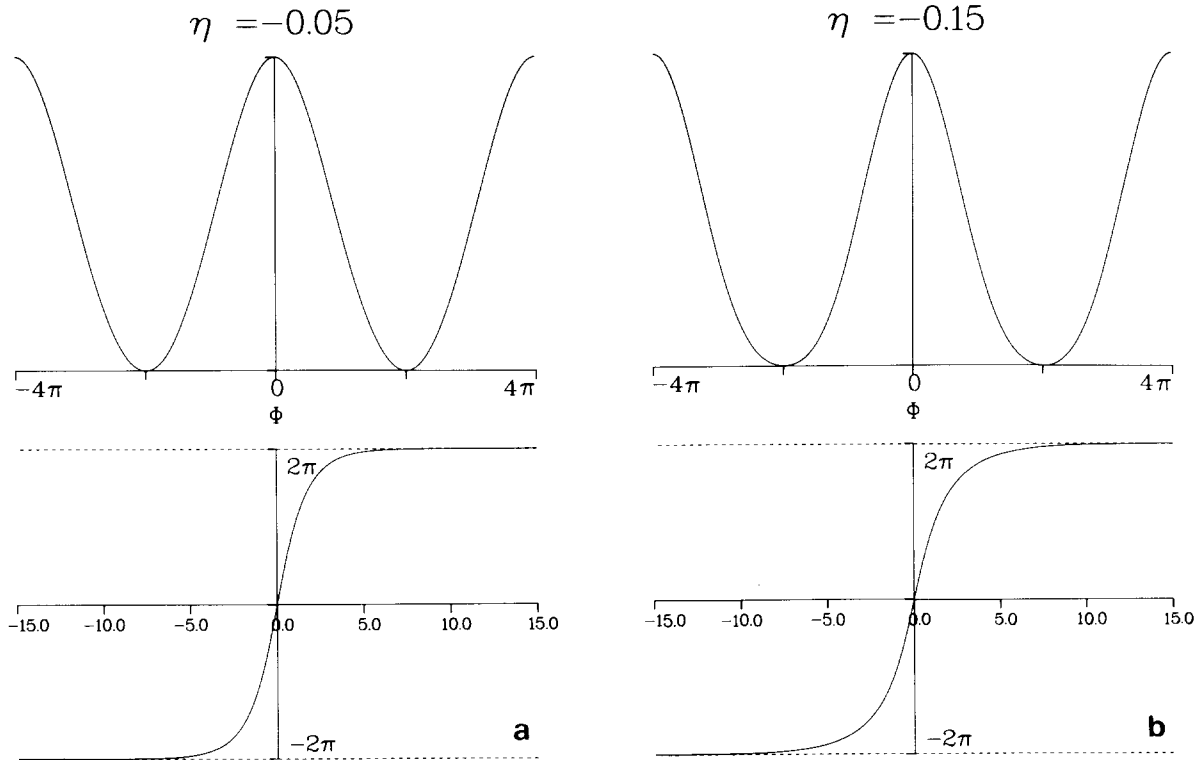$$\eta = -0.05$$

$$\eta = -0.15$$

Fig. 13. a) A plot of the DSG potential and the single kink solution for $\eta = -0.05$. b) A plot of the DSG potential and the single kink solution for $\eta = -0.15$.
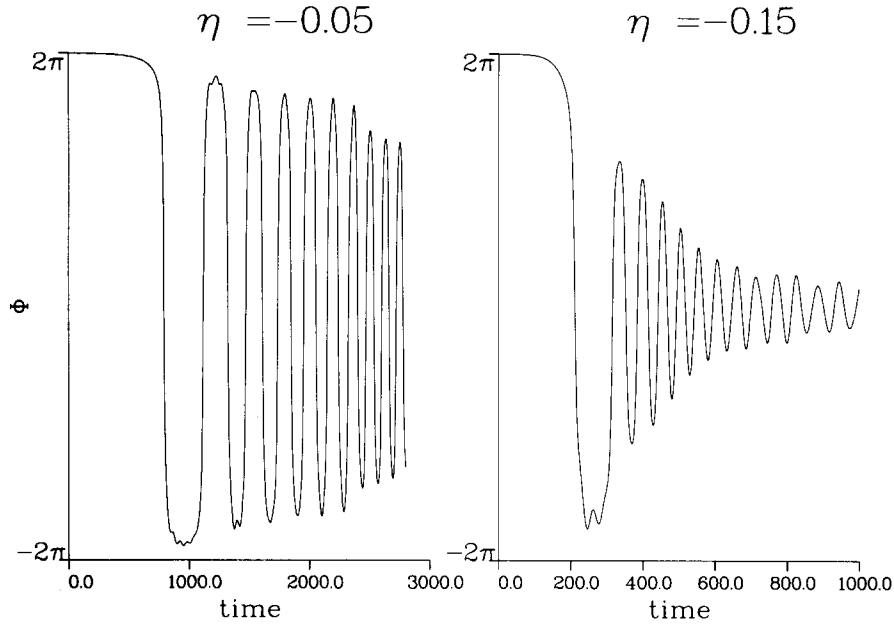
$$\eta = -0.05 \qquad\qquad \eta = -0.15$$

Fig. 14. A plot versus time of $\phi(x = 0, t)$ illustrating the nature of the oscillatory final state formed in $K\overline{K}$ collisions: a) for $\eta = -0.05$, where $v_c = 0.112$, a collision with v less than v_c (here $v = 0.07$) leads to a long-lived, slowly decaying state; b) for $\eta = -0.15$, where $v_c = 0.390$, a collision with v less than v_c (here $v = 0.350$) leads to a rapidly decaying state.

velocities for trapping ($v_c = 0.112$ for $\eta = -0.05$, $v_c = 0.390$ for $\eta = -0.15$) we have observed only localized, decaying oscillatory states. No resonances were seen. Although it is impossible for us to exclude entirely the existence of very narrow resonance regions, we can assert that if present this structure is on a very fine scale indeed.

There is one striking qualitative difference between the decaying, oscillatory final states observed for $v < v_c$ for the two values of η. For $\eta = -0.05$, this state survives for a very long time, with the "amplitude" – defined as the maximum of $\phi(x = 0, t)$ over a single period – decaying roughly linearly in time. In sharp contrast, for $\eta = -0.15$, the amplitude of the oscillatory state decays rather rapidly, apparently following an exponential law. This difference is very clearly illustrated in fig. 14.

It is possible to understand this difference semi-quantitatively in terms of the existence or non-existence of stable "breather" solutions to the DSG for different values of η [31, 39]. To be specific, let us consider the expansion of $V_{DSG}(\phi)$ around its minimum value for $|\eta| < \frac{1}{4}$. In terms of

$\theta \equiv \phi - 2\pi$ one finds for $\theta \approx 0$

$$V_{DSG}(\theta) = \frac{-4}{1 + |4\eta|}\left[1 + \eta - \frac{1}{2}\theta^2\left(\frac{1 + 4\eta}{4}\right)\right.$$
$$\left. + \frac{\theta^4}{24}\left[\frac{1 + 16\eta}{16}\right] + \cdots\right]. \tag{4.1}$$

Hence keeping nonlinear terms up through θ^4 in V_{DSG} yields the field equation

$$\frac{d^2\theta}{dt^2} - \frac{d^2\theta}{dx^2} + \left(\frac{1 + 4\eta}{1 + |4\eta|}\right)\theta$$
$$- \left(\frac{1 + 16\eta}{24(1 + |4\eta|)}\right)\theta^3 = 0. \tag{4.2}$$

The search for "breather" – i.e., nonlinear, spatially localized, time-periodic – solutions to eq. (4.2) can be handled by standard asymptotic perturbation theory methods [40–43]. Expanding

$$\theta(x, t) = \varepsilon\left(\Psi(X, T)e^{i\tau} + \Psi^*(X, T)e^{-i\tau}\right), \tag{4.3}$$

with

$$\tau = \left(\frac{1 + 4\eta}{1 + |4\eta|} \right)^{1/2} t, \quad T = \varepsilon^2 \tau,$$

and

$$X = \varepsilon \left(\frac{1 + 4\eta}{1 + |4\eta|} \right)^{1/2} x,$$

one obtains, after equating powers of ε, a nonlinear Schrödinger equation for the envelope function, Ψ, of the form

$$2i \frac{\partial \Psi}{\partial T} - \frac{\partial^2 \Psi}{\partial X^2} - K|\Psi|^2 \Psi = 0, \quad (4.4)$$

where $K = (1 + 16\eta)/[8(1 + 4\eta)]$. Eq. (4.4) will have spatially localized soliton solutions, and hence eq. (4.2) will have breather solutions, *only* for $K > 0$. Thus the dividing line for the existence of stable, small amplitude breathers for $|\eta| < \frac{1}{4}$ is $\eta > -\frac{1}{16}$. For values of $\eta > -\frac{1}{16}$, one finds the explicit breathers solution in terms of the original variables to be $[\frac{1}{4} > \eta > -\frac{1}{16}]$

$$\phi(x, t) = 2\pi + 2\varepsilon \operatorname{sech} \frac{\varepsilon x}{4} \left(\frac{1 + 16\eta}{1 + |4\eta|} \right)^{1/2} (s)$$

$$\times \cos \left[\left(\frac{1 + 4\eta}{1 + |4\eta|} \right)^{1/2} t \left(1 - \frac{\varepsilon^2(1 + 16\eta)}{32(1 + 4\eta)} \right) \right].$$

$$(4.5)$$

The interpretation of our data is thus that for $\eta = -0.05$, one is in the range for which stable breathers can exist, and hence the oscillatory state formed in K$\overline{\text{K}}$ collisions being "near" a stable solution decays very slowly, whereas for $\eta = -0.15$, since there are no stable breathers, the corresponding trapped K$\overline{\text{K}}$ state decays much more rapidly. Of course, the analytic breather solution in (4.5) is valid for small amplitude, ε, whereas the oscillatory states formed in the K$\overline{\text{K}}$ collisions have large amplitude (see fig. 14). Nonetheless, numerical simulations in the closely related ϕ^4 model [43]

suggest that the large amplitude, (apparently) stable breathers, which connect smoothly with the analytic small amplitude solution, do exist.

5. Kink–antikink scattering for $\eta > 0$

5.1. General properties of the kinks

As previously mentioned, for positive values of η two different regions can be distinguished, according to the topology of the DSG potential. For $0 < \eta < \frac{1}{4}$, the potential is topologically similar to the SG potential, while for $\eta > \frac{1}{4}$ the tops of the potential barriers are replaced by local minima, as indicated in fig. 1. These local minima are responsible of the existence of an additional unstable solution [2]. Since we are interested here in topological kink solutions connecting two adjacent *absolute* minima of the potential, we shall treat these two regions simultaneously. It is interesting to observe that, in the domain $\eta > 0$, the DSG potential can be written in terms of a new parameter R which has a natural physical interpretation. Specifically, one has

$$V(\phi) = -\frac{4}{\cosh^2 R} \left(-\cos \phi/2 \right.$$

$$\left. + \frac{1}{4} \sinh^2 R \cos \phi - 1 - \frac{1}{4} \sinh^2 R \right). \quad (5.1)$$

Apart from the term introduced for convenience to insure that $V(\phi)$ vanishes at the absolute minima ($\phi = 2\pi + 4n\pi$), this expression is equivalent to eq. (1.3) used previously if η is expressed as

$$\eta = \frac{1}{4} \sinh^2 R. \quad (5.2)$$

Eq. (5.2) shows that this new parametrization is indeed valid only for positive η. As noted in section 2, for $\eta > 0$ there is only one type of kink interpolating between two absolute minima of the potential. In terms of the parameter R the static kink (antikink) solution has a very simple form,

$$\phi_{K(\overline{K})}(x) = 2n(2\pi) \pm 4 \tan^{-1} \frac{\sinh(x)}{\cosh(R)}. \quad (5.3)$$

Interestingly, this solution can be expressed in terms of two sine-Gordon soliton solutions,

$$\phi_{K(\bar{K})}(x) = 2n(2\pi)$$
$$\pm [\phi_{SGK}(x + R) - \phi_{SGK}(R - x)], \qquad (5.4)$$

where

$$\phi_{SGK}(x) = 4\tan^{-1}\exp(x). \qquad (5.5)$$

Eq. (5.4) shows clearly the physical meaning of the parameter R: the DSG kink can be considered as the superposition of two (bound) sine-Gordon solitons centered at $\pm R$ and thus separated by the distance $2R$. Fig. 15 shows the shape of the DSG potential (5.1) and the corresponding kink solutions for various values of R ($R = 0.5$, 1.2, 2.4, and 10 which correspond respectively to $\eta = 0.136$, 0.567, 14.960, and 3.023×10^7). The meaning of R is graphically demonstrated in fig. 15: when R is small ($R < 1$) the DSG kink appears only as a slightly distorted 4π kink but at large R ($R = 10$) the DSG kink is split into two sine-Gordon-like 2π kinks. This property appears also in the expression of the kink energy as a function of R,

$$E(R) = 16\left(1 + \frac{2R}{\sinh 2R}\right). \qquad (5.6)$$

In the limit $R \to 0$, the model tends to a pure SG model with period 4π and kink energy $E(0) = 32$, while in the limit of large R the DSG model tends to a pure SG model of period 2π. In the later case, the DSG kink tends to a pair of SG solitons and its energy is $E(R \to \infty) = 2 \times 8 = 16$, as shown by eq. (5.6).

Although for large R the DSG kink looks like two SG kinks (that we shall henceforth designate 'subkinks') the two subkinks are *not* free to move with respect to each other. Their equilibrium spacing is approximately given by $2R$. When the DSG kink moves, the two subkinks perform identical (in phase) translations. In terms of the small oscillations around the kink waveform, this overall translation corresponds to the "Goldstone mode" of

the 4π kink. In addition to this "in phase" translation, one can expect an "out of phase" motion, in which the relative distance between the two subkinks changes [44]. This observation was already used by Hudák [19], who analyzed this oscillation in the limit of large subkink separation (our large R limit) in terms of the distance between the subkinks. Since we are interested here in $K\bar{K}$ scattering, in which small oscillations around the kink waveform have been shown to play a major role, we have solved numerically for all values of R the Schrödinger-like eq. (2.6) which describes these small oscillations. The results are summarized in fig. 16 in terms of parameter R. In addition to the continuum starting at $\omega_0 = 1$ independently of R and to the $\omega = 0$ Goldstone mode, we found a localized shape mode of the kink. Its frequency is very close to 1 for small R and decreases to 0 when R becomes large. Fig. 17 shows the Schrödinger potential $V_{SCH}(x)$ and the corresponding eigenfunctions of the shape mode for several values of R. Although we have not been able to solve this equation analytically for all values of R, we have carried out a perturbation analysis in the two limits $R \to 0$ and $R \to \infty$. Using the solution (5.4), the potential $V_{SCH}(x)$ given by eq. (2.7) is obtained as

$$\frac{d^2 V(\phi)}{d\phi^2}\bigg|_{\phi = \phi_K(x)}$$
$$= -1 + \tanh^2 R \cos\phi - \frac{1}{\cosh^2 R}\cos\frac{\phi}{2}$$
$$= -1 + \tanh^2 R\left[2\frac{\cosh^2 R - \sinh^2 x}{\cosh^2 R + \sinh^2 x} - 1\right]$$
$$- \text{sech}^2 R\left[\frac{\cosh^2 R - \sinh^2 x}{\cosh^2 R + \sinh^2 x}\right]. \qquad (5.7)$$

As usual, the corresponding Schrödinger equation admits $d\phi_K/dx$ as a zero energy (Goldstone) mode. Using (5.4), its (unnormalized) eigenfunction is obtained as

$$\psi_0(x) = \phi_0(x + R) + \phi_0(R - x), \qquad (5.8)$$
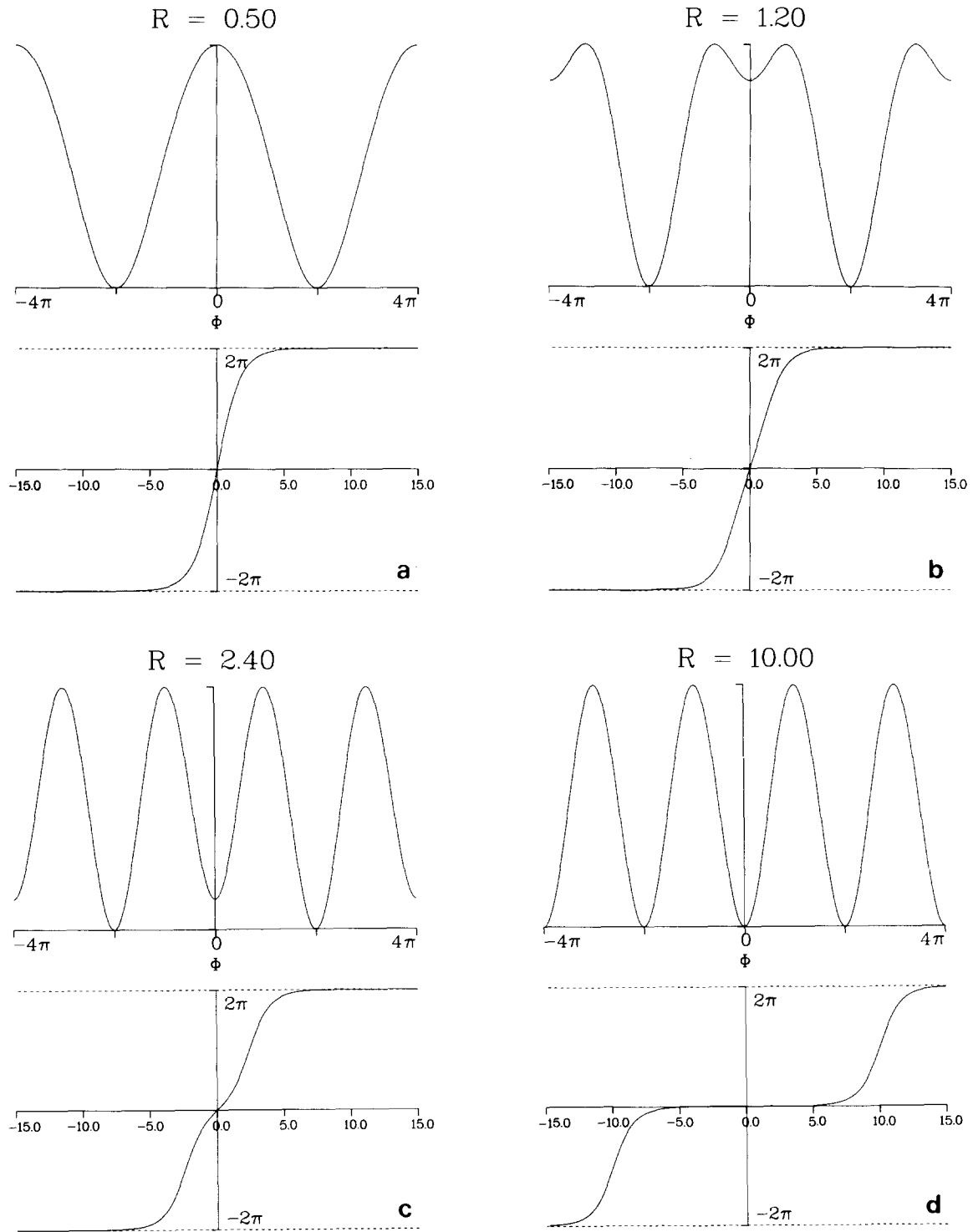
R = 0.50

R = 1.20

R = 2.40

R = 10.00

Fig. 15. The DSG potential and kink solutions for different values of R: a) $R = 0.5$ ($\eta = 0.136$); b) $R = 1.20$ ($\eta = 0.567$); c) $R = 2.40$ ($\eta = 14.94$); d) $R = 10$ ($\eta = 3.023 \times 10^7$).
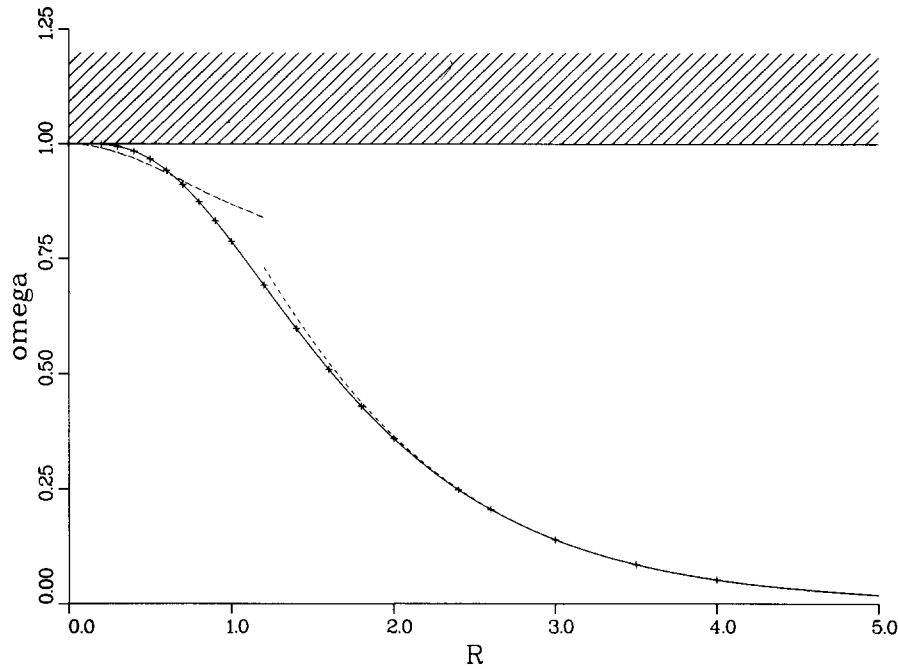
Fig. 16. The spectrum of the small oscillations around the DSG kink in the domain $\eta > 0$ as a function of the parameter R. The continuum starts at $\omega = 1$. The full line shows the frequency ω_s of the shape mode (numerical result). The dashed line shows the frequency of the shape mode obtained for large R from the odd combination of the Goldstone modes of the 'subkinks'. The dotted line shows the frequency of the shape mode obtained from perturbation of the lowest state in the continuum of the SG model corresponding to $R = 0$.

where

$$\phi_0(x) \equiv \frac{d\phi_{SGK}}{dx} = 2 \operatorname{sech}(x) \qquad (5.9)$$

is the Goldstone mode of the sine-Gordon kink.

This result has an immediate and illuminating interpretation in terms of an analogy to quantum mechanics; this analogy is appropriate, of course, because of the previously noted formal similarity of eq. (2.7) to the Schrödinger equation. Consider fig. 17d. The Schrödinger potential has a clearly separated "double well" form and thus one expects that the ground state wave function – i.e., the Goldstone mode – would have a wave function *approximately* given by the *sum* of the individual ground state wave functions for the two separate potential wells. Eq. (5.8) shows that this result is *exactly* true, for all R. The same analogy suggests that, for large R, the first excited state of V_{SCH}

should (1) be very close in energy to the $\omega = 0$ ground state and (2) have a wave function, $\psi_1(x)$, given *approximately* by the *difference* between the two individual ground state wave functions:

$$\psi_1(x) \approx \phi_0(x + R) - \phi_0(x - R)$$

$$\equiv \frac{d\phi_K(x)}{dR}. \qquad (5.10)$$

Note that fig. 16 shows that, indeed, for large R the first excited state of V_{SCH} *does* approach the ground state ($\omega = 0$). Note further that the final equality in (5.10) indicates that this first excited state is, as expected, the *shape* mode of the 4π kink, in that it is related to the *relative* motion of the two subkinks. Thus henceforth we shall use the notation $\psi_s(x) \equiv \psi_1(x)$.

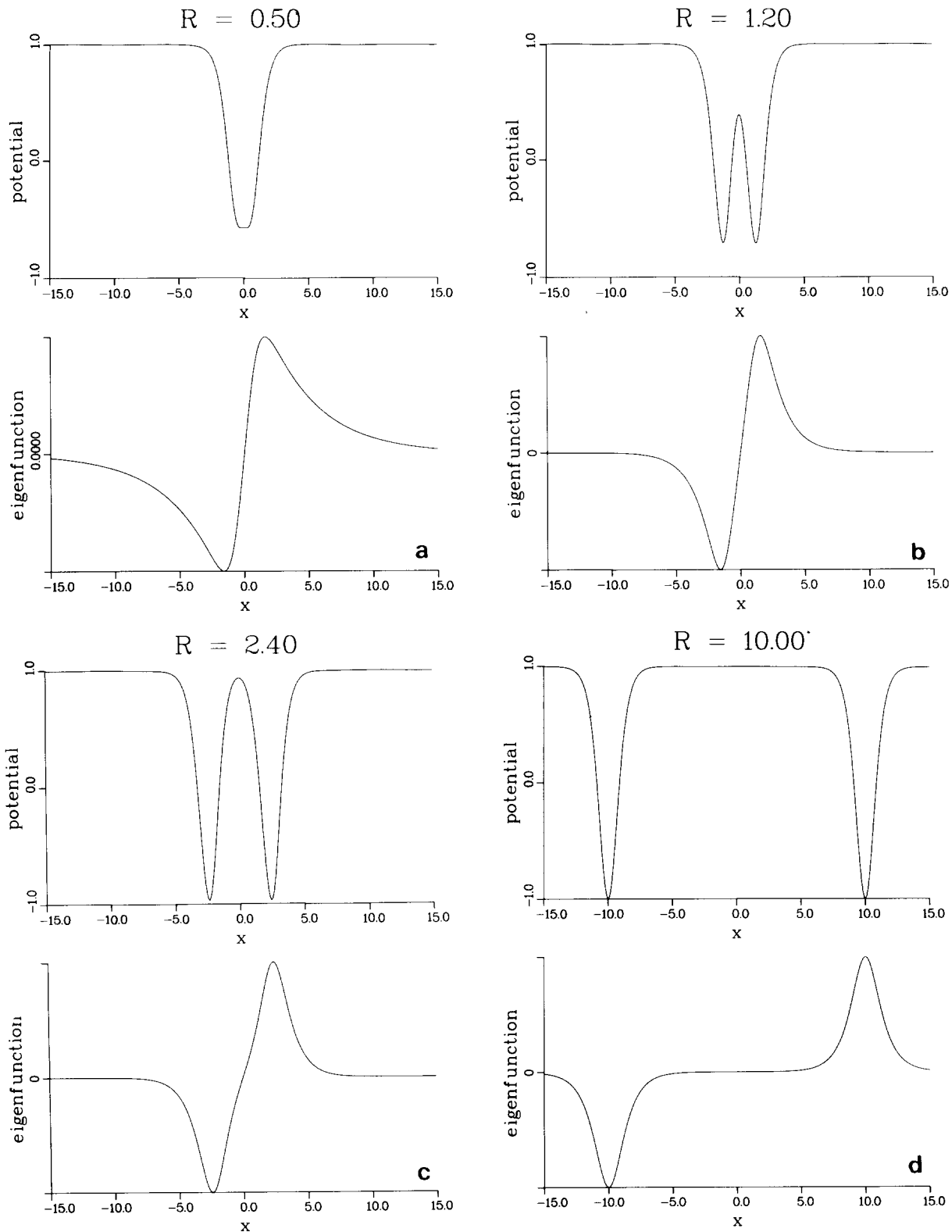Taking $\psi_s(x)$ as given by eq. (5.10), normalizing properly and evaluating the energy corresponding

Fig. 17. The potential of the "Schrödinger" equal describing the small oscillations around the kink and the eigenfunction of the shape mode (for various values of R): a) $R = 0.50$; b) $R = 1.20$; c) $R = 2.40$; d) $R = 10.0$.

to this approximate solution we find

$$\tilde{\omega}_{\mathrm{s}}(R) \equiv \left\langle \psi_{\mathrm{s}}(x) \left| \frac{-\mathrm{d}^2}{\mathrm{d}x^2} + V_{\mathrm{SCH}} \right| \psi_{\mathrm{s}}(x) \right\rangle$$

$$/\left\langle \psi_{\mathrm{s}}(x) | \psi_{\mathrm{s}}(x) \right\rangle \qquad (5.11a)$$

$$= \frac{3}{\sinh^2 R} - \frac{1}{\cosh^2 R} \frac{\sinh 2R + 2R}{\sinh 2R - 2R}. \qquad (5.11b)$$

The variation of $\tilde{\omega}_{\mathrm{s}}(R)$ is plotted in fig. 16 (dashed line) together with the actual value $\omega_{\mathrm{s}}(R)$ obtained numerically. As expected $\tilde{\omega}_{\mathrm{s}}(R)$ gives a very good estimate of $\omega_{\mathrm{s}}(R)$ for large R. Moreover, fig. 16 shows surprisingly that $\tilde{\omega}_{\mathrm{s}}(R)$ is rather accurate even for R as small as $R \approx 1$, for which the individuality of the subkinks has disappeared. Of course, $\mathrm{d}\phi/\mathrm{d}R$ will not give an accurate estimate of ω_{s} or of the shape of the eigenfunction for very small R. Such estimates can, however, be obtained if one looks for perturbations of the continuum eigenstates of the SG model obtained in the limit $R \to 0$. Let us define $A = 1/\cosh^2 R$. The potential $V_{\mathrm{SCH}}(x)$ given by eq. (5.7) can be expressed around $R = 0$ ($A = 1$) as

$$V_{\mathrm{SCH}}(A, x) = V_{\mathrm{SCH}}(1, x) + (A - 1)$$

$$\times \frac{\mathrm{d}}{\mathrm{d}A} V_{\mathrm{SCH}}(A, x)|_{A=1} + \mathcal{O}(A - 1)^2. \qquad (5.12)$$

In this expression $V_{\mathrm{SCH}}(1, x)$ is the potential describing the small oscillations around the sine-Gordon soliton, so that

$$V_{\mathrm{SCH}}(1, x) = -2 \operatorname{sech}^2(x) \qquad (5.13)$$

and the perturbative term is obtained as

$$\frac{\mathrm{d}}{\mathrm{d}A} V_{\mathrm{SCH}}(A, x) \bigg|_{A=1} = \frac{8 \sinh^2 x - 2}{\cosh^4 x}. \qquad (5.14)$$

Under the perturbation (5.14) the energy of the Goldstone mode of the SG system that exists for $R = 0$ is *not* shifted whereas the energy of the lowest energy state ($k = 0$) in the continuum, the

eigenfunction of which is

$$u_0(x) = \frac{1}{\sqrt{2\pi}} \tanh x,$$

is shifted by

$$\Delta E = (A - 1) \frac{4}{3\pi} = \frac{4}{3\pi} \left(\frac{1}{\cosh^2 R} - 1 \right).$$

The energy of this perturbed state is then

$$\omega_{\mathrm{s}}''^2(R) = 1 - \Delta E. \qquad (5.15)$$

As shown in fig. 16 (dotted line) this expression gives an estimate of the shape mode frequency which is valid only for very small values of R. Thus the shape mode of the DSG model for $\eta > 0$ evolves as R increases from a perturbation of the lowest state of the SG model obtained for $R = 0$ to the antisymmetric combination of the two SG-like Goldstone modes of the subkinks for large R.

Let us now turn our attention to $\mathrm{K}\overline{\mathrm{K}}$ scattering. Since the model tends to a sine-Gordon model in the two limits $R \to 0$ and $R \to \infty$, we expect only elastic scattering with a vanishing critical velocity in these two limits. That we observe this numerically is shown in fig. 18. A maximum in the critical velocity is observed for $R \approx 1$ where $v_{\mathrm{c}} = 0.24$. Two points should be emphasized about these results. First, although it is not very far from $R = 0.8813$ ($\eta = \frac{1}{4}$), the maximum in the critical velocity does *not* correspond to occur at $\eta = \frac{1}{4}$, and thus this maximum does not seem to be related to the change in structure (the appearance of the additional minimum) of the potential. Indeed, a similar 'anomaly' in the critical velocity has already been observed in PC for the generalized SG model [45], in which no such change of shape occurs. A theoretical determination of the position of the maximum of the critical velocity would require a complete description of the mechanism of the $\mathrm{K}\overline{\mathrm{K}}$ interaction during the collision process; this is beyond our present understanding. Second, the maximum critical velocity in the region $\eta > 0$ is $v_{\mathrm{c}} = 0.24$ and for most $\eta > 0$ v_{c} is
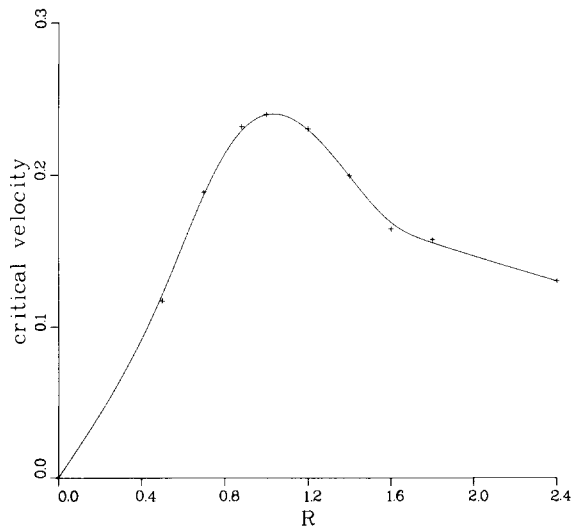
Fig. 18. The variation of the critical velocity in $K\overline{K}$ collisions in the region $\eta > 0$ as a function of R.

much less than 0.24. This value has to be compared with $v_c \approx 0.36$ for $\eta = -1$. We have already noticed [31] that when kinks pass through each other, v_c is found to be smaller than when they reflect. This fact seems to be quite general but, again, its quantitative understanding would require a detailed description of the collision process.

5.2. $K\overline{K}$ Scattering for various values of R

We now consider in detail $K\overline{K}$ scattering for various values of R. We shall see that in the region $\eta > 0$ the DSG model gives rise to an extremely rich variety of interactions between kinks and antikinks. In the intermediate domain $R \approx 1$, processes similar to those observed previously for $\eta < -\frac{1}{4}$, and now well understood, take place. In this sense the region $R \approx 1$ is the simplest one, and we shall thus consider it first. We consider then the ranges of small R and large R where new phenomena appear.

5.2.1. $K\overline{K}$ scattering for $R = 1.2$

For this value of R (corresponding to $\eta = 0.567$), the frequency of the shape mode is $\omega_s = 0.69204$. Fig. 19 shows the final velocity as a function of the

initial velocity in $K\overline{K}$ scattering. One recognizes in this figure the resonant structures already discussed for $\eta < -\frac{1}{4}$. The critical velocity is here $v_c = 0.2305$, and the inset in fig. 19 shows that, for $v > v_c$, the kink and antikink pass through each other; this is as expected for this sine-Gordon-like model. For $v < v_c$, ten "two-bounce" resonances were observed. Note that, as shown in the inset in fig. 19, the process is here similar to that previously observed in PC: the two kinks pass through each other a first time but cannot escape to infinity since $v < v_c$. They come back, passing through each other a second time before escaping to infinity if the resonance condition is fulfilled. The net result of the resonance is thus a reflection of the two kinks, as in the case $\eta < -\frac{1}{4}$, although the scattering process is qualitatively different. Nonetheless, as we have shown in PC, the "resonant energy exchange mechanism" developed for resonances in ϕ^4-like models still applies. Table VII lists the observed resonances and shows that they are very well explained by the general theory presented in section 3 (eq. (3.5)). The indices of the observed resonances vary between 2 and 12. The mean value of the product $T_2 \times (v_c^2 - v_{n_2}^2)^{1/2}$ is found to be $\beta = 2.418$. The velocities for $v > v_c$ evolve according to eq. (3.3) with $\alpha = 1.98$ which yields the theoretical value $\beta = 2.23$, according to eq. (3.4b). Thus the two-bounce resonant exchange theory is again found to be in reasonable agreement with the numerical observations and, in particular, determines very well the positions of the resonances if we use the 'experimental value' of β in eq. (3.5).

Although both on general grounds and in view of the results of section 3 we would expect higher (three-, four-, ...) bounce resonances, these were not observed in our simulations. Several comments are in order at this point. First, in view of limitations of computer time, we were not able to carry out a systematic search for these higher resonances. Second, the two-bounce resonances for $\eta > 0$ are already quite narrow; thus, for instance, the width of the resonance of index 3 for $R = 1.2$ is $\Delta v = 1.25 \times 10^{-3}$ whereas for $\eta = -0.50$ one must go to the index 5 resonance before a similarly
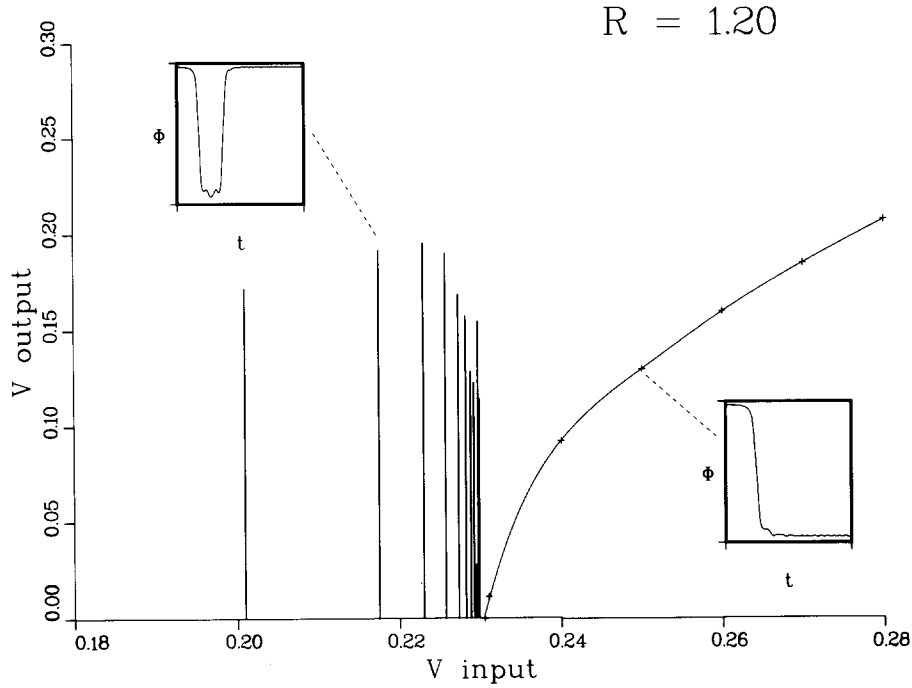
$$R = 1.20$$

Fig. 19. The outgoing velocities (V output) as a function of the initial velocities (V input) in $K\overline{K}$ collisions for $R = 1.2$. The vertical lines below v_c indicate the resonances in which the K and $\overline{K}$ separate after two collisions. Note that no widths are shown for the resonances. The nature of the $K\overline{K}$ collision is indicated by the insets, which show $\phi(x = 0, t)$ versus t.

Table VII

Analysis of the two-bounce resonances in $K\overline{K}$ scattering for $R = 1.2$

Position of resonance v_{n_2}	Final velocity v_f	Time between the 1st & 2nd interactions T_2	$T_2(v_c^2 - v_{n_2}^2)^{1/2}$	$\omega_s T_2/2\pi$	Index, n_2	Theoretical v_{n_2}
0.2010	0.1721	21.55	2.447	2.373	2	0.20538
0.2175	0.1918	31.05	2.404	3.419	3	0.21820
0.2230	0.1954	39.80	2.378	4.384	4	0.22328
0.2257	0.1954	49.05	2.383	5.402	5	0.22581
0.2273	0.1688	59.40	2.402	6.542	6	0.22726
0.2282	0.1578	68.90	2.412	7.588	7	0.22816
0.2288	0.1287	78.5	2.421	8.646	8	0.22876
0.2292	0.1228	87.75	2.432	9.665	9	0.22918
0.2295	0.0280	97.30	2.444	10.761	10	0.22949
0.2297	0.1549	105.90	2.458	11.664	11	0.22972
0.22985	0.1147	113.40	2.454	12.490	12	0.22990

small width ($\Delta v = 1.9 \times 10^{-3}$) is encountered. Recalling that the resonance widths fall as $1/n^3$, one sees that this difference is significant. Since the $\eta > 0$ two-bounce resonances are already quite narrow, the higher bounce structures, if present,

are expected to be extremely narrow and thus very difficult to observe. Finally, particularly in anticipation of our forthcoming results, we must note that for $\eta > 0$ the energy transfer from the translational motion into the shape mode seems

less efficient and well-defined than for $\eta < -\frac{1}{4}$. This is clearly indicated by the relatively low value of the critical velocity for $\eta \geq 0$. In particular, although we did not have sufficient data to make an accurate separation, it appears that shape mode-translation mode energy transfer here was considerably less elastic than for $\eta < 0$ with the lost energy going into non-localized continuum modes. If the collisions are sufficiently inelastic, one would expect the resonance structures to disappear, with the higher bounce structure being more sensitive. More specifically since for *both* $R \to 0$ and $R \to \infty$ the DSG approaches (different) SG theories, for both large and small R one can describe the system as a weakly perturbed SG model. Hence, based on previous experience, we anticipate that even the two-bounce resonance structure will disappear for $R < R_{min}$ *and* for $R > R_{max}$, where R_{min} and R_{max} remain to be determined. Indeed, in the ensuing subsections, we shall see that this is the case.

5.2.2. $K\overline{K}$ scattering at small R ($R = 0.5$)

The value $R = 0.5$ corresponds to $\eta = 0.136$, and the shape mode frequency is $\omega_s = 0.96692$ in this case. As shown in fig. 15a the potential shape is very close to sinusoidal, and consequently the model is quite close to a pure SG model. The critical velocity is found to be 0.117, which indicates that the energy removed from the kinks' kinetic energy in a $K\overline{K}$ scattering is very small. In spite of a careful search, we have *not* observed any resonant scattering in this case: that is, for $v < v_c$, the kinks appear always to be trapped. Since there *is* a shape mode here – albeit quite near the continuum – this result disagrees with a naive application of the resonant energy exchange mechanism. However, since the naive theory ignores inelasticity, in view of our previous remarks on the weakly perturbed SG system, we feel this result is not surprising. That the basic energy exchange mechanism still exists is shown by the fact that $K\overline{K}$ scattering exhibits properties which are reminiscent of the resonant scattering observed for larger values of R. In particular, for $v < v_c$, the

time T_3 between the second and third interaction of the trapped $K\overline{K}$ pair does *not* evolve monotonically with v. Recall that if a resonant scattering *were* to exist, the time T_3 would become infinite at velocities v_{n_2} corresponding to two-bounce resonances, because the K and $\overline{K}$ would never come back after their second collision. Here, instead of becoming infinite, T_3 exhibits well-defined maxima at particular velocities that we label v'_n in fig. 20. The positions of these maxima are listed in table VIII. From this table we see that the velocities v'_n can be determined by eq. (3.5), in a manner similar to the velocities v_n corresponding to resonances. These velocities v'_n correspond to 'quasi-resonances', as previously observed in PC in a case where the shape mode was absent. The origin of these quasi-resonances can be understood qualitatively in a manner similar to real resonances. The only difference is that, even if the resonance condition is fulfilled *exactly* when $v = v'_n$, the energy restored to the $K(\overline{K})$ translational motion after the second collision is *not* sufficient to allow the kinks to escape to infinity. Nonetheless, because the energy is partially restored at resonance, the kinks do escape to a large separation before returning to collide again; this behavior is reflected in the maxima observed in T_3, which occur, as expected, when the resonance condition (3.1) is satisfied.

5.2.3. $K\overline{K}$ scattering at large R ($R \geq 1.4$)

When R is increased beyond $R = 1.2$ the numerical results exhibit three particular features:

i) a gradual disappearance of the resonances (for $1.4 \leq R \leq 1.8$);

ii) the appearance of a new type of quasi-resonance apparently involving states in the continuum (for $R = 2.4$);

iii) the appearance of a qualitatively new feature in $K\overline{K}$ interactions (for $R \geq 1.4$).

Let us examine now these points. Consider first the gradual disappearance of the resonances as R increases. As R is increased from $R = 1.2$, fig. 18 shows that the critical velocity decreases significantly: for $R = 1.4$ $v_c = 0.1996$, for $R = 1.6$
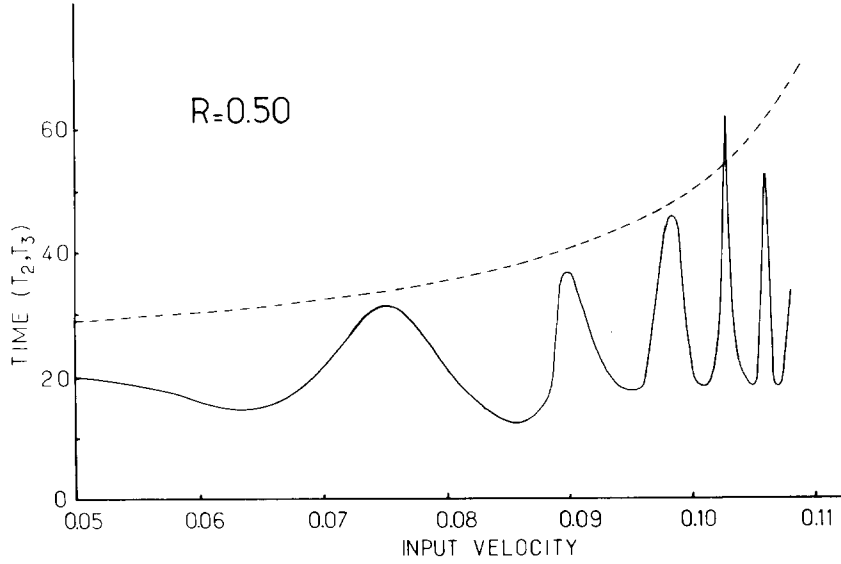
Fig. 20. The time T_2 between the two first $K\overline{K}$ collisions (dashed line) and time T_3 between the 2nd and 3rd $K\overline{K}$ collisions (full line) as a function of the input velocity in $K\overline{K}$ collisions for $R = 0.50$. The maxima in T_3 correspond to 'quasi-resonances'.

Table VIII
Analysis of the quasi-resonances in $K\overline{K}$ scattering for $R = 0.5$

Position of quasi-resonance v_{n_2}	Time T_2	Time T_3	$\beta = T_2(v_c^2 - v_{n_2}^2)^{1/2}$	$\omega_s T_2/2\pi$	Index n	Theoretical v_{n_2}
0.050	28.84	19.86	3.058	4.434	4	0.0406
0.0752	33.84	31.53	3.042	5.208	5	0.0762
0.0900	40.56	36.80	3.045	6.242	6	0.0902
0.0980	47.09	44.04	3.027	7.248	7	0.0979
0.1029	54.00	61.80	3.024	8.310	8	0.1026
0.1060	60.58	50.00	3.028	9.322	9	0.1057

$v_c = 0.1647$, and for $R = 1.8$ $v_c = 0.1577$. Simultaneously resonances become harder and harder to observe in the numerical simulations. Table IX lists the resonances observed for $R = 1.4$ and $R = 1.6$. We have detected only 3 of them for $R = 1.4$ and 2 for $R = 1.6$. In the case $R = 1.8$ we have been unable to observe any resonant scattering. The resonances, when they exist, are still well explained by the general resonant energy exchange mechanism as shown in table IX. A study of the widths of the resonances (table X) shows that they decrease rapidly when R increases; this indicates

that the resonance condition is becoming increasingly difficult to fulfill in the sense that sufficient energy for escape is transferred only for a very small range of velocities. As previously mentioned, this is the case if a significant part of the initial kinetic energy is transferred into nonlocalized modes rather than into the shape mode: that is, if the shape mode-translation mode interactions are inelastic. Again only a detailed description of the collision process, going beyond the energy exchange mechanism that we consider, can explain quantitatively this result. Nevertheless, a strong

Table IX
Analysis of the two-bounce resonances in $K\overline{K}$ scattering for $R = 1.4$ and $R = 1.6$

Position of reso-nance v_{n_2}	Final velocity, v_f	Time between the 1st & 2nd interactions T_2	$\beta = T_2(v_c^2 - v_n^2)^{1/2}$	$\omega_s T_2/2\pi$	Index n_2	Theoretical v_{n_2}
$R = 1.4$, $v_c = 0.1996$, $\omega_s = 0.5978$						
0.1725	0.1681	23.71	2.381	2.256	2	0.17500
0.1880	0.1680	35.44	2.376	3.372	3	0.18788
0.1930	0.1467	46.70	2.377	4.443	4	0.19273
$R = 1.6$, $v_c = 0.1647$, $\omega_s = 0.5095$						
0.1420	0.1231	27.68	2.309	2.245	2	0.14428
0.1560	0.1215	40.99	2.165	3.324	3	0.15516

indication that this "inelasticity" does indeed underlie the observed behavior comes from the study of $K\overline{K}$ interaction for $R = 2.4$.

For $R = 2.4$ a *new* type of quasi-resonance appears. This value of R corresponds to $\eta = 14.94$, and the shape mode has the frequency $\omega_s = 0.24822$. The critical velocity in the $K\overline{K}$ interaction is found to be quite low, $v_c = 0.1305$. The study of the $K\overline{K}$ scattering for $v < v_c$ gives results qualitatively very similar to those observed for $R = 0.5$. Specifically, we detect no resonances, but we do observe quasi-resonances, for which the time T_3 between the second and third collisions is maximal. These quasi-resonances are listed in table XI, and fig. 21 shows the variation of T_2 and T_3 as a function of the input velocity in this case. The velocities v_n' corresponding to these quasi-resonances are again well described by a formula like eq. (3.5) as shown in table XI but *with a frequency $\omega_s' = 1.0456$ instead of the frequency 0.24822 of the shape mode.* This result suggests that, for this large value of R the dominant energy exchange is not occurring via the shape mode, but via an excited state of the kinks *which lies in the continuum.* Such a state is not localized around the kinks and consequently we observe quasi-resonances instead of resonances because the energy disperses. Similar quasi-resonances via a state lying in the continuum were already observed in PC in a case where no shape mode existed.

Table X
Widths of some resonances for two different values of R

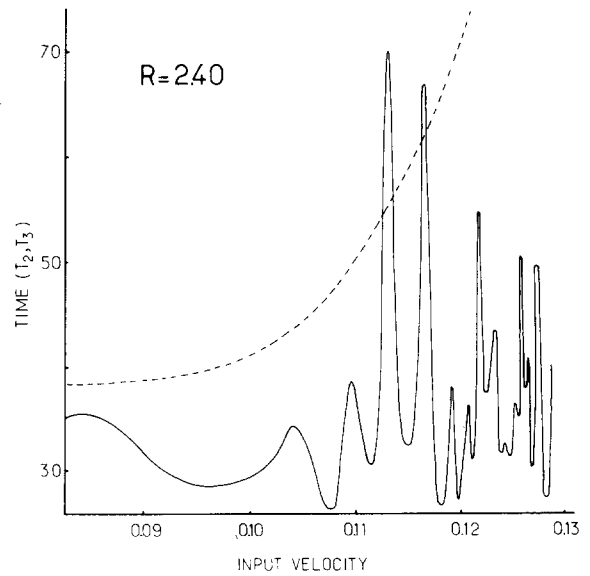|	$R = 1.2$	$R = 1.6$
$n = 2$	$\Delta v = 4.25 \times 10^{-3}$	$\Delta v = 2.25 \times 10^{-3}$
$n = 3$	$\Delta v = 1.50 \times 10^{-3}$	$\Delta v = 0.80 \times 10^{-3}$

Fig. 21. The time T_2 between the two first $K\overline{K}$ collisions (dashed line) and time T_3 between the 2nd and 3rd $K\overline{K}$ collisions (full line) as a function of the input velocity in $K\overline{K}$ collisions for $R = 2.40$. The maxima in T_3 correspond to 'quasi-resonances'.

Table XI
Analysis of the quasi-resonances in $\overline{K}K$ scattering for $R = 2.4$

Position of quasi-resonance v_n	Time T_2	Time T_3	$\beta = T_2(v_c^2 - v_n^2)^{1/2}$	$\omega_s T_2/2\pi$	Index n	Theoretical v_n
0.050	34.10	31.50	4.110	5.567	5	0.0635
0.085	38.07	35.70	3.769	6.335	6	0.0884
0.104	43.32	34.38	3.419	7.209	7	0.1007
0.110	49.80	37.90	3.464	8.287	8	0.1082
0.1135	56.35	50.26	3.629	9.377	9	0.1130
0.1165	62.21	66.91	3.658	10.353	10	0.1165
0.1190	67.86	37.90	3.634	11.293	11	0.1189
0.1205	74.03	36.30	3.709	12.320	12	0.1208
0.1215	79.16	56.71	3.742	13.173	13	0.1223
0.1230	86.22	43.50	3.759	14.348	14	0.1234
0.1240	91.35	32.21	3.715	15.202	15	0.1243
0.1251	101.50	37.90	3.479	16.891	16	0.1251
0.1255	105.60	50.4	3.778	17.573	17	0.1257
0.1262	111.70	41.00	3.612	18.588	18	0.1262
0.1267	118.80	35.20	3.721	19.770	19	0.1266
0.1270	124.70	49.70	3.743	20.752	20	0.1270

At present, we have no quantitative explanation for this result, but several qualitative observations are worth making. First, similar quasi-resonances apparently involving a state in the continuum were observed in PC, albeit in a case in which no shape mode existed. Second, the apparent lack of excitation of the shape mode in this case is consistent with the increasing inelasticity of shape mode-translation mode collisions which we have postulated as the mechanism for the disappearance of the resonance structure for $R \leq 1.8$. Third, although one might naively expect that with the shape mode so clearly isolated from the continuum, resonances would be stronger, from the very close agreement (shown in fig. 16) between $\omega_s(R)$ and $\tilde{\omega}_s(R)$ (see (5.11)) for $R = 2.4$, it is clear that the "shape" mode is in fact very well described by the antisymmetric combination of the Goldstone modes for the two subkinks. Thus the subkinks are beginning to assert their independent existence, and the $\overline{K}K$ collision process is approaching a *sequence* of subkink interactions. Since the individual subkinks are sine-Gordon-like (i.e., have *no* shape modes), it is not at all surprising that the elasticity of the shape mode-translational mode interaction falls rapidly. Finally, it is important to state clearly that, as in PC, we have *no* explanation for the apparent selection of a *particular* continuum mode; this remains an open problem.

In addition to the disappearance of resonances and the presence of quasi-resonance structures, for $R \geq 1.4$, a qualitatively new feature appears in $\overline{K}K$ scattering. To understand this new feature, let us first describe the features which are *not* novel. For $v < v_c$ in the region $R > 0$, the two-bounce resonant scatterings occur as shown in fig. 22; the kinks pass through each other twice, escaping to infinity after the second interaction. Non-resonant scattering leads to the formation of an oscillatory, breather-like state, as shown in fig. 23. These processes are familiar from our previous studies. Here, however, in essence because of the subkink structure of the DSG for $R > 0$, we find an additional process. For example, in fig. 24, we illustrate a final state in which *two counter-propagating breathers* are formed! Note that the initial condition here ($v = 0.154$) is quite similar to that ($v = 0.156$) in fig. 22, and yet the final state is dramatically different. A *qualitative* understanding of this "breather pair" formation comes, as hinted
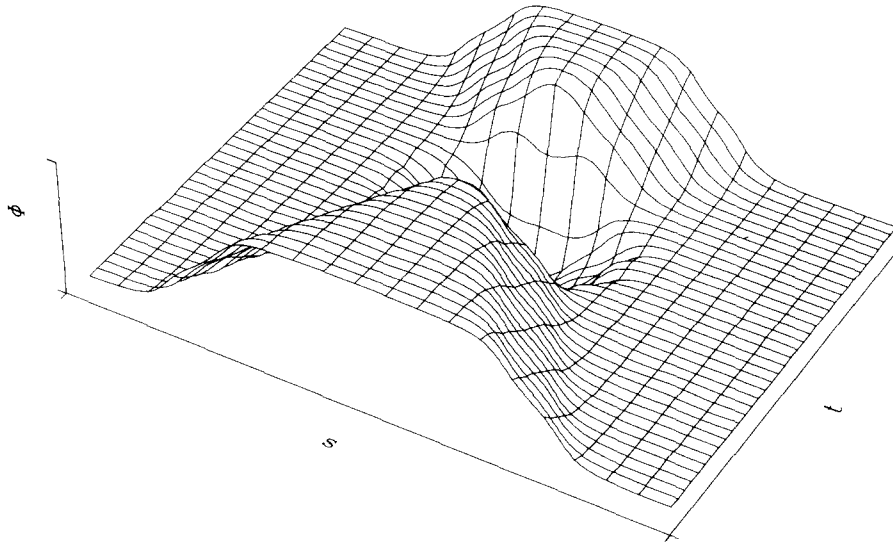
R = 1.60   v = 0.156

Fig. 22. A perspective plot of the system ($\phi(x)$) at different times during a $K\overline{K}$ collision for $R = 1.60$ for an input velocity corresponding to a resonance. (In this and all subsequent perspective plots, the initial state is at the top of the figure.)
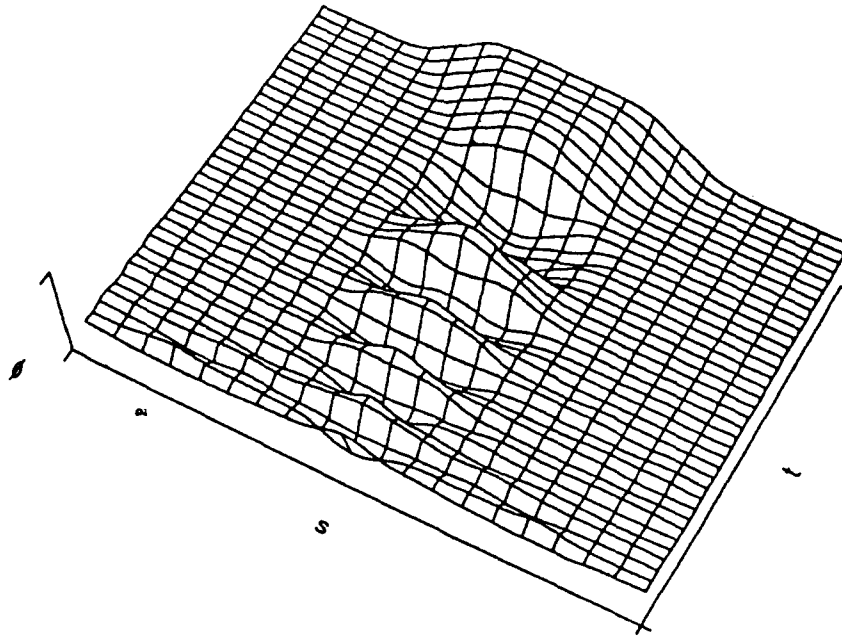

Fig. 23. A perspective plot of the system at different times during a $K\overline{K}$ collision which produces a trapping of the two DSG kinks (breather-like state) ($R = 1.40$, $v = 0.180$).

$$R = 1.60 \quad v = 0.154$$
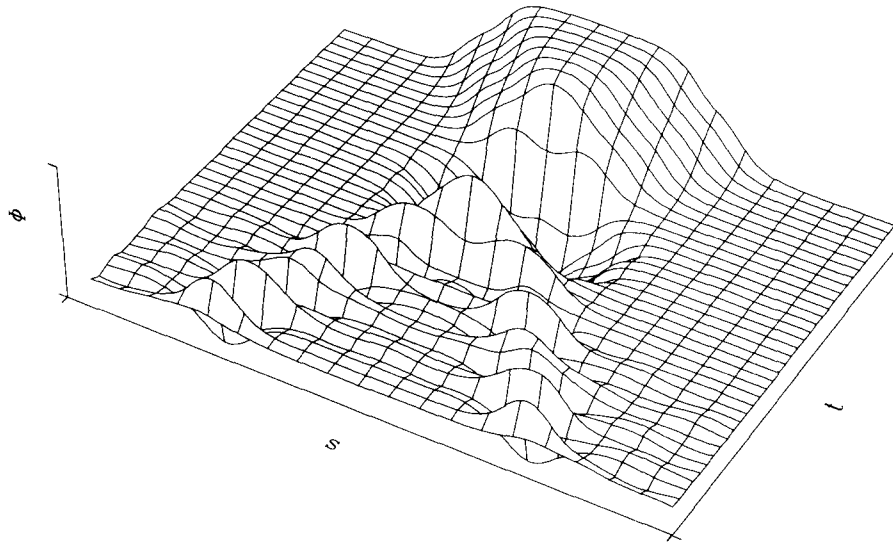
Fig. 24. A perspective plot of the system at different times during a $K\overline{K}$ collision at $R = 1.60$, $v = 0.154$. The collision produces two breathers, which escape from the collision point.
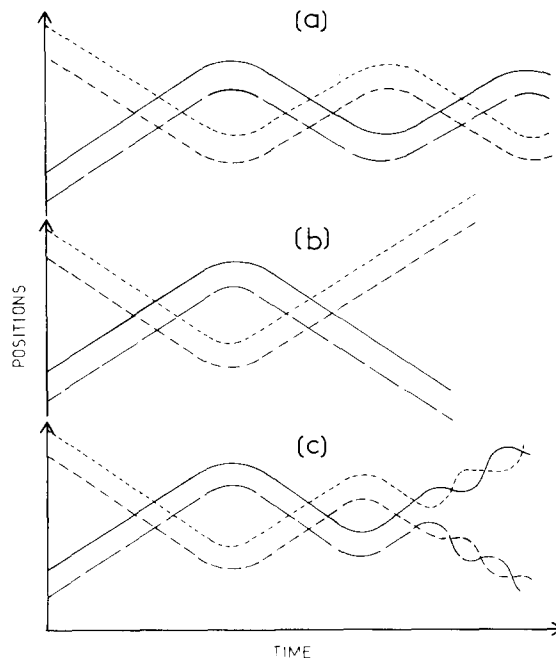
(a)

(b)

(c)

TIME

Fig. 25. A schematic plot of the positions of the subkinks in different types of $K\overline{K}$ collisions observed for $R = 1.40$ and 1.60 (figs. 22 to 24). Each subkink is represented by a particular type of line so that its trajectory can be followed in the different collisions. The variations of the velocities of the subkinks due to their different interactions are, for reasons of clarity, not indicated in this figure.
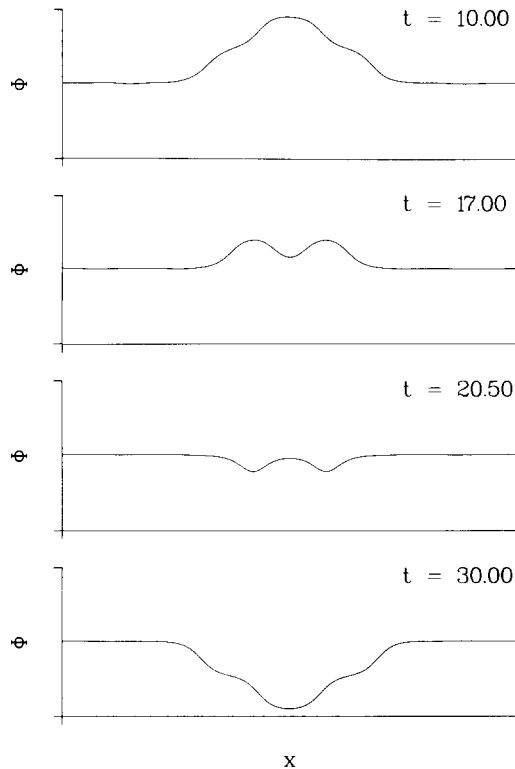
Fig. 26. Plots of a $K\overline{K}$ collision for $R = 2.4$ at different times of the collision. The two kinks pass through each other.

Fig. 27. The effective $K\overline{K}$ interaction potential in the DSG model for various values of R. For small R the potential well corresponds to the usual $K\overline{K}$ attraction in the SG theory. At large R the interaction between individual subkinks appears as additional wells.

above, from considering the subkink structure of the DSG kinks. In fig. 25 we have plotted schematically the variation versus time of the positions of the subkinks in $K\overline{K}$ collisions of the DSG model for the three types of final states previously mentioned: a) breather like final state (fig. 23); b) resonant scattering (fig. 22); and c) formation of two breathers escaping to infinity (fig. 24). The two-first cases are simple and very similar to that observed in ϕ^4 (CSW) or modified SG (PC) because the two subkinks which constitute a DSG kink remain bound to each other when the DSG kinks pass through each other. This is no longer true in c): the two DSG kinks pass through each other twice without being separated into their subkinks, but on their third collision only *one* of the two subkinks of each DSG interchanges while the second one does not. That such a mechanism in terms of subkinks is reasonable is indicated in
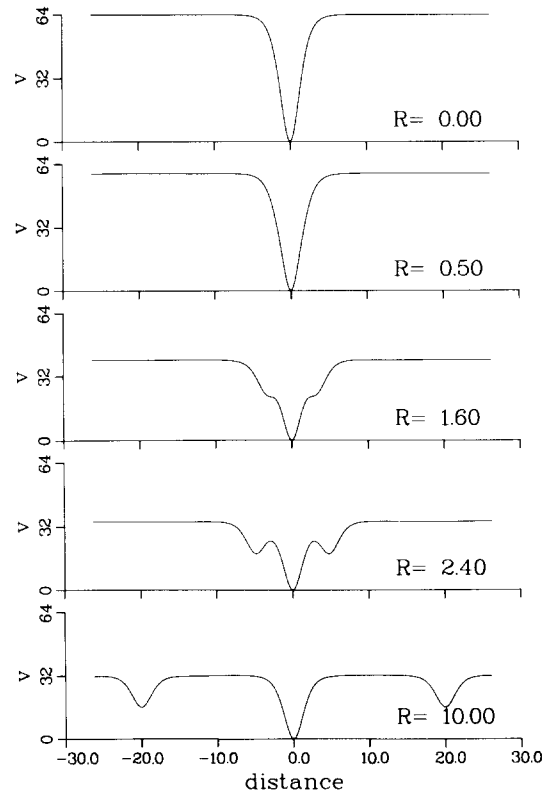
fig. 26, which shows the details of a $K\overline{K}$ collision for $R = 2.4$. There are clearly four steps in the collision shown in fig. 26:

1) the DSG K and $\overline{K}$ approach each other. The order of the individual subkinks can be denoted by $S1\,S'1{:}\overline{S'2}\,\overline{S2}$ where Si $(\overline{Si})$ represents a subkink of kink (antikink) i;

2) the two central subkinks pass through each other. The order is now $S1\,\overline{S'2}\,S'1\,\overline{S2}$;

3) the subkinks in the two lateral pairs $S\overline{S}$ pass through each other to give $\overline{S'2}\,S1\,\overline{S2}\,S'1$;

4) the two subkinks in the central pair $S\overline{S}$ pass through each other to complete the collision process, yielding give $\overline{S'2}\,\overline{S2}\,S1\,S'1$.

The $K\overline{K}$ collision which produces the two breathers escaping to infinity shown in fig. 24

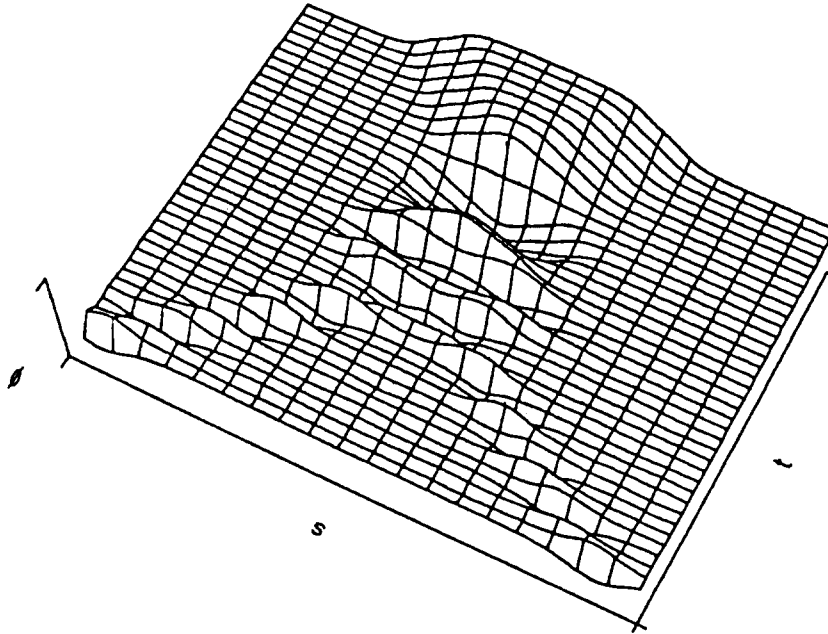Fig. 28. A perspective plot of the $K\overline{K}$ collision for $R = 1.4$, $v = 1.70$ showing the system at different times.

involves the same three first steps. However, after step three, the $\overline{S'}2\,S1$ and $\overline{S}2\,S'1$ subkink/anti-subkink pairs remain trapped, thus producing the two counterpropagating breathers observed in fig. 23; a schematic view of this process is shown in fig. 25c. That such a process can occur is motivated qualitatively both by our numerical observations and by analytic results [43] that for a *perturbed* sine-Gordon system, $K\overline{K}$ collisions can lead to breather formation. In essence, the process in fig. 24 can be viewed as two sine-Gordon systems, each perturbing the other just enough to allow the $K\overline{K}$ to trap. Of course, for such a picture to be even qualitatively valid, the separate subkinks must exhibit considerable individuality. Although fig. 26 provides a visual indication of this individuality, to obtain a more quantitative estimate we have evaluated numerically the $K\overline{K}$ interaction potential [30, 31] for the DSG model. As previously [30, 31], this potential can be estimated as a function of the $K\overline{K}$ separation, $2y$, by inserting into the DSG Hamiltonian the *Ansatz*

$$\phi_A(x, 2y) \equiv \phi_K(x + y) + \phi_{\overline{K}}(x - y). \qquad (5.16)$$

This potential, evaluated numerically, is shown in fig. 27 as a function of the separation $2y$ for various values of R. When R is very small, we recover the familiar single potential well corresponding to the usual attractive $K\overline{K}$ interaction in the sine-Gordon theory, but when R increases, two additional side wells appear. Finally, the potential splits into three separate wells, the central one being twice as deep as the lateral ones. These simply correspond to the two separate interactions of the subkinks (lateral wells) and to the complete interaction involving simultaneously the two subkinks (central well). Thus, the individuality of the two subkinks which compose the DSG solution does appear to be sufficiently established, for $R \gtrsim 1.4$, to be responsible for the feature in which the initial DSG kink can be broken into two parts.

At the risk of moving from physics to zoology, let us mention one additional, related process, as illustrated in fig. 28. This case was observed for $R = 1.4$, $v = 1.70$. At a first glance, fig. 28a which shows the state of the system at different times looks very similar to fig. 24 apart from a more
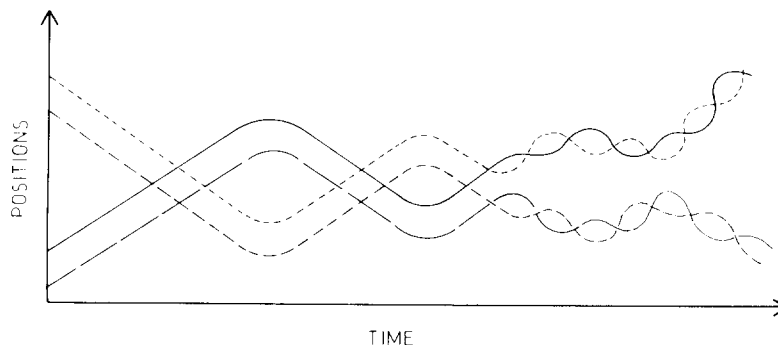
Fig. 29. Schematic plot of the motion of the subkinks in the collision of fig. 28. The two DSG kinks collide twice and produce two breathers which collide again before escaping to infinity.

complicated interaction before the two breathers are formed. Figure 29b 'decodes' the details of the interaction: it appears that, as in the case presented in fig. 24, two breathers are formed after the third $K\overline{K}$ collision but are unable to escape to infinity. So they come back, collide again and only then escape to infinity! This case points out the possibility of *resonant structures in breather collisions*. To study such a possibility quantitatively would require having a (non-integrable) theory in which breather solutions were accurately known. Further, in view of the "natural" oscillation frequency of the breathers, the resonance condition, if it existed, would presumably be quite involved. We are thus quite happy, at present, to leave these as open problems.

Finally, as the above discussions and figs. 15 and 27 suggest, at very large R the subkinks behave increasingly like SG solitons; they exhibit weaker and weaker interactions (as indicated by small v_c's) and the DSG kinks are able to pass through each other completely for all but the smallest velocities.

6. Summary and conclusions

Given the several different topological forms of the double sine-Gordon potential as a function of η, it is perhaps not surprising that the interactions of the kinks and anti-kinks in this theory exhibit a wide range of interesting phenomena. Indeed, al-

though we have focussed solely on the resonance structure in $K\overline{K}$ scattering – and, for $\eta < -\frac{1}{4}$, on "small" kinks only – we have nonetheless observed several different types of behavior. In nearly all cases, the "resonant energy exchange" mechanism provides an explanation of this behavior; in most cases, it also provides a detailed, quantitative fit. For two values of $\eta < -\frac{1}{4}$, for example, we studied the now familiar [30, 31] "two-bounce" resonances in considerable detail. In this region, the DSG theory is like the ϕ^4 model [30] in that the kinks, if they escape, reflect from each other. In the case of $\eta = -0.50$, we were able to study systematically resonances involving higher bounces for the first time. Here again the resonant energy exchange mechanism provided a quantitative fit and, in addition, gave a natural explanation for the occurrence of the $(n + 1)$-bounce resonances at the edge of the n-bounce resonances and for the great difference in "scale factors" – α and β – between the two- and three-bounce resonances. The observed "resonance upon resonance" structure is somewhat reminiscent of self-similar behavior observed in certain chaotic dynamical systems. One must be careful, however, in carrying this analogy too far. Most importantly, it must be recognized that, by assuming conservative energy exchange between the shape and translation modes, the resonant energy exchange mechanism neglects all coupling to the small oscillations – the "radiation" – which also exist in the full equation. This coupling, which is responsible for much of the inelasticity observed

in $K\overline{K}$ collisions above the first trapping velocity, leads to the eventual breakdown of the assumption of conservative energy exchange and thus to the extinction of the very high order resonances.

The region $-\frac{1}{4} < \eta < 0$ provided a different test of the theory, in that in this region there is no shape mode associated with the kink and thus, we predict no resonances. Although "null result" physical experiments can only really be discussed in terms of confidence levels, we did *not* observe any resonances. Interestingly, we did discover a substantial difference between the nature of the trapped oscillatory state formed below the critical velocity for $\eta = -0.15$ and $\eta = -0.05$. We explained this behavior in terms of the existence/non-existence of a "breather" oscillation; for $\eta > -\frac{1}{16}$, asymptotic perturbation theory predicts such a breather, whereas for $\eta < -\frac{1}{16}$, no small-amplitude breather exists.

For $\eta > 0$, by introducing a parameter R such that $\eta = \frac{1}{4} \sinh^2 R$, we showed that the individual DSG kinks could, loosely speaking, be thought of as two bound sine-Gordon kinks separated by a distance $2R$. This interpretation led naturally to an explanation of the shape oscillation of the DSG kink as the "optical" (or counter-motion) mode of the two bound subkinks. For a wide range of R, this explanation provided a quantitative fit.

In general, in this region the KK interactions were "sine-Gordon-like", in the sense that above the critical velocity the kinks pass through each other, rather than reflecting. Consistent with previous results [31], this meant that the $K\overline{K}$ interactions were in general weaker than for $\eta < 0$; for example, the maximum value of v_c for $\eta > 0$ is $\approx 0.24\ldots$, much less than that for, say, $\eta = -0.50$ ($v_c \approx 0.345\ldots$) or $\eta = -1.00$ ($v_c = 0.359\ldots$). For $R = 1.2$ ($\eta = 0.567\ldots$) we observed two-bounce resonances in quantitative agreement with the theory. Higher bounce resonances were not observed, probably because of their extreme narrowness (if they exist). For very small R ($= 0.5$, so that $\eta = 0.136$) we did not observe actual resonances, although "quasi-resonances" – that is, values of v for which the time between interaction exhibited

sharp peaks – were observed. In our view the absence of true resonances is explained by the smallness of the energy transfer to the shape mode, which allows other, from our perspective, "inelastic" processes (eg., coupling to radiation) to drain off sufficient energy to prevent the resonant restoration of energy to the translation mode.

For increasing R (> 1.4), we observe the gradual disappearance of the resonances, consistent again with the observed decrease in v_c and overall weakening of the interaction. We also observed several new features, for which we have at best qualitative explanations. For $R = 2.4$, we found quasi-resonances apparently involving states in the continuum. For R in the range 1.4–1.6, we observed very complicated interactions (involving the subkinks), including the production of counter-propagating breathers as a final state!

Although in any of the several physical contexts of the DSG we would expect the fine details of our numerical results to be washed out, the central idea that one can envision the DSG kinks – be they domain walls, optical pulses, or twists in polymeric chains – as deformable particles, capable of storing energy in their internal structure, should remain valid. In particular, as discussed in CSW, the use of collective coordinates – the two describing the shape and translation modes, for example – to approximate the behavior of the full (infinite degree of freedom) partial differential equation deserves further investigation. We stress that this reduction to a few "effective" modes is directly related to similar mode reductions seen in pattern selection and long-time asymptotics studies. These collective coordinate approaches to $K\overline{K}$ scattering, as well as the issue of a more rigorous mathematical understanding of the entire resonant energy exchange theory, remain important open problems.

Acknowledgements

for valuable discussions on various aspects of this work. The hospitality of the Laboratories O.R.C. at the Université de Dijon is gratefully acknowledged by DC and PS, as is that of the Center for Nonlinear Studies at Los Alamos by MP and PS. This work was supported in part by the USDOE.

References

[1] This equation establishes our conventions for the normalization of the field ϕ and of the potential. The overall factor in the potential can, of course, be altered by scaling the space and time variables.

[2] C.A. Condat, R.A. Guyer and M.D. Miller, Phys. Rev. B27 (1983) 474–494. For additional details on the properties of the potential and the nature of the solutions for all η, readers should consult this reference.

[3] K. Maki and Pradeep Kumar, Phys. Rev. B14 (1976) 118, 3920; K. Maki, Physics 90B (1977) 84.

[4] P.W. Kitchenside, R.K. Bullough and P.J. Caudrey, pp. 291–296 in: Solitons in Condensed Matter Physics, A.R. Bishop and T. Schneider, eds. (Springer, Berlin, 1978); pp. 254–265 in: Structural Stability in Physics, W. Güttinger and H. Eikemeir, eds. (Springer, Berlin, 1979); Physica Scripta 20 (1979) 673.

[5] R.K. Bullough, P.J. Caudrey and H.M. Gibbs, pp. 107–141 in: Solitons, R.K. Bullough and P.J. Caudrey, eds. (Springer, Berlin, 1980).

[6] R.K. Dodd, R.K. Bullough and S. Duckworth, J. Phys. A8 (1975) L64.

[7] S. Duckworth, R.K. Bullough, P.J. Caudrey and J.D. Gibbon, Phys. Lett. 57A (1976) 19.

[8] R.K. Bullough, P.J. Caudrey, J.D. Gibbon, S. Duckworth, H.M. Gibbs, B. Bölger and L. Baede, Optics Communications 18 (1976) 200.

[9] H.J. Mikeska, J. Phys. C11 (1978) L29.

[10] K.M. Leung, Phys. Rev. B26 (1982) 226; B27 (1983) 2877.

[11] H.J. Mikeska, J. Phys. C13 (1980) 2913.

[12] R. Boudreau and A. Caillé, Solid State Comm. 47 (1983) 783.

[13] Rahul Pandit and C. Tannous, Phys. Rev. B28 (1983) 281; Rahul Pandit, C. Tannous and J.A. Krumhansl, Phys. Rev. B28 (1983) 289.

[14] M. Steiner and J.K. Kjems, p. 191 in: Solitons and Condensed Matter Physics, A.R. Bishop and T. Schneider, eds. (Springer, Berlin, 1978).

[15] R. Dingle, M.E. Lines and S.L. Holt, Phys. Rev. 187 (1969) 643.

[16] For recent reviews see P. Bak, Reports on Prog. in Phys. 45 (1982) 587 and L.A. Turkevich and S. Doniach, Ann. of Phys. 139 (1982) 343. Briefly, a commensurate/incommensurate phase transition can be viewed as result from a competition between two natural lengths in the system. As a relevant example, consider the competition between a solid state lattice with equilibrium spacing "a" subjected to an externally applied potential of period "b". The system can behave quite differently in the cases where a and b are commensurate or incommensurate.

[17] T. Munakata, J. Phys. Soc. Japan 52 (1983) 1635.

[18] S. Iwabuchi, Prog. Theor. Phys. 70 (1983) 941.

[19] O. Hudák, J. Phys. C16 (1983) 2641 and 2659; O. Hudák and L. Trlifaj, J. Phys. A18 (1985) 445.

[20] S. Iwabucki and H. Fukuyama, J. de Phys. Colloq. C3 44 (1983) C3-1001.

[21] A.J. Hopfinger, A.J. Lewanski, T.J. Sluckin and P.L. Taylor, in: Solitons and Condensed Matter Physics, A.R. Bishop and T. Schneider, eds. (Springer, Berlin, 1978); H. Duey-Aharon, T.J. Sluckin, P.L. Taylor and A.J. Hopfinger, Phys. Rev. B21 (1980) 3700.

[22] R.M. DeLeonardis and S.E. Trullinger, Phys. Rev. B27 (1983) 1867.

[23] A. Luther, p. 78 in: Solitons and Condensed Matter Physics, A.R. Bishop and T. Schneider, eds. (Springer, Berlin, 1978).

[24] D.W. Kitchenside, A.L. Mason, R.K. Bullough and P.J. Caudrey, pp. 54–57 in: Solitons and Condensed Matter Physics, A.R. Bishop and T. Schneider, eds. (Springer, Berlin, 1978).

[25] E. Magyari, Phys. Rev. B29 (1984).

[26] K. Saermark, "Double sine-Gordon Equation with Damping Term. Some Exactly Solvable Cases," preprint, Technical Univ. of Denmark, 1984.

[27] J. Schiefman and P. Kumar, Physica Scripta 20 (1979) 435.

[28] P. Kumar and R.R. Holland, p. 229 in: Nonlinear Problems: Present and Future, A.R. Bishop, D.K. Campbell and B. Nicolaenko, eds. (North-Holland, Amsterdam, 1982).

[29] H. Segur, J. Math. Phys. 24 (1983) 1439.

[30] D.K. Campbell, J.F. Schonfeld and C.A. Wingate, Physica 9D (1983) 1.

[31] M. Peyrard and D.K. Campbell, Physica 9D (1983) 33.

[32] S. de Lillo and P. Sodano, Lett. al Nuovo Cimento 37 (1983) 380.

[33] After the calculations for the present paper were completed, we discovered that O. Hudák (ref. 19) had introduced a similar parametrization and, more importantly, had carried out a closely related analysis of the small oscillations around the kink for large R. Nonetheless, since this analysis is important for our interpretation of the $K\bar{K}$ scattering, for clarity and completeness we present an abbreviated discussion of this point in section 5.

[34] It is, of course, possible to multiply the potential by a scale factor, singular at $\eta = -\frac{1}{4}$, which is chosen such that $V'' \neq 0$ for $\eta = -\frac{1}{4}$. This is done in ref. 22. Nonetheless, the point $\eta = -\frac{1}{4}$ remains special since the scaled potential becomes infinitely high and only a particular limiting procedure allows the small kink to continue to exist.

[35] In ref. 28, the authors study $K\bar{K}$ scattering for a *range* of values of $\eta < -\frac{1}{4}$, and in particular determine, as a function of η, the critical velocity for the trapping of a "small"

$K\overline{K}$ pair to a breather state (for $-0.31 \geq \eta \geq -3.6$) and the critical velocity for conversion of a "small" $K\overline{K}$ pair to a "large" $K\overline{K}$ pair (for $-0.83 > \eta \geq -3.6$).

[36] Although readers should refer to CSW (and references therein) for details of the calculation of the $K\overline{K}$ potential, we can motivate its form and properties intuitively by considering a simple topological argument. We *define* the $K\overline{K}$ "potential", $V_{K\overline{K}}(x_0)$, as being the energy of the static field configuration consisting of a kink at $+x_0$ and an antikink at $-x_0$. Clearly for $x_0 \to +\infty$, this "potential" goes to $2E_K$. For $x_0 \to 0$, the K and $\overline{K}$ cancel each other totally, and so the energy is zero. For $x_0 \to -\infty$, the energy depends on whether kinks are allowed topologically to pass through each other, as in the sine-Gordon theory, or are *not* allowed to do so, as in ϕ^4. In the former case $V_{K\overline{K}}(x_0) \to_{x \to -\infty} 2E_K$, while in the latter $V_{K\overline{K}}(x_0)$ increases without limit as $x_0 \to -\infty$. In any event, we see that there is always a region, for $x_0 \approx 0$, with lower energy than two regions for $x_0 \to \pm\infty$. Hence the K and $\overline{K}$ have a mutually attractive potential.

[37] On the discrete chain the continuum form of ϕ_K^I is, of course, not exact. However, for kinks which are 20 particles ($= 20$ "lattice units") wide, the discreteness effects are very small. For example, the actual velocity of propagation on the discrete lattice differs from the nominal input velocity by $\Delta v \approx 10^{-5}$.

[38] Limitations of computer time meant that we did not attempt to observe three bounce resonances in the region *above* the $n = 17$ two bounce resonance. Given the success of our interpretation for the $n = 14$ case, we feel quite confident that these three bounce resonances are there.

[39] Here we have made minor changes in the notation used in CSW to avoid possible confusion with our current notation.

[40] M. Remoissenet, to be published, studies a wide class of nonlinear scalar field theories in one spatial dimension and derives conditions for the existence of stable, small amplitude breathers.

[41] For a pedagogical discussion of these asymptotic methods, see chap. 2 in Alan C. Newell, Solitons in Mathematics and Physics, CBMS Lectures (No. 48) (SIAM, Philadelphia, 1984).

[42] R.F. Dashen, B. Hasslacher and A. Neveu, Phys. Rev. D11 (1975) 3424.

[43] D.K. Campbell and J.W. Negele, to be published.

[44] For an interesting consequence of this "composite" nature of the DSG solitons for large R see A.C. Newell, Jour. Math. Phys. 18 (1977) 922.

[45] M. Remoissenet and M. Peyrard, Phys. Rev. B29 (1984) 3153.

[46] D.J. Kaup and A.C. Newell, Proc. Roy. Soc. London A361 (1983) 413.